Determination of ice interface temperature, sublimation rate and the dried product resistance, and its application in the assessment of microcollapse using through-vial impedance spectroscopy

Yowwares Jeeraruangrattana[a], Geoff Smith[b]*, Evgeny Polygalov[b], Irina Ermolina[b]

[a] *Research and Development Institute, The Government Pharmaceutical Organization (GPO), Thailand*

[b] *Leicester School of Pharmacy, De Montfort University, The Gateway, Leicester, LE1 9BH, United Kingdom*

**Corresponding author*

Journal	European Journal of Pharmaceutics and Biopharmaceutics
Date Submitted	January 27,2020
Date revised	April 15, 2020
Date Accepted	April 22, 2020

Cite as:

Jeeraruangrattana, Y., Smith, G., Polygalov, E. and Ermolina, I., 2020. Determination of ice interface temperature, sublimation rate and the dried product resistance, and its application in the assessment of microcollapse using through-vial impedance spectroscopy. European Journal of Pharmaceutics and Biopharmaceutics, 152, pp.144-163.

Abstract

Through-vial impedance spectroscopy (TVIS) is a new approach for characterizing product attributes during freeze-drying process development. In this study, a pair of copper foil electrodes was attached to the external surface of a Type I glass tubing vial, of nominal capacity 10 mL and containing 3.5 g of an aqueous solution of 5% w/v lactose, and the impedance spectrum of the vial and contents recorded during a lyophilization cycle. The cycle included a temperature ramp in the primary drying stage in order to induce a collapse event in the dry layer. Using the peak in the dielectric loss spectrum, associated with the dielectric relaxation of ice, methods were developed to predict the sublimation rate and the ice interface temperature at the sublimation front, from which the dry layer resistance was then calculated. A four-fold increase in sublimation rate and a reduction in the dry layer resistance was observed once the the ice interface temperature reached −33 °C, which coincides with the onset of the glass transition (as determined by DSC) and the time point at which micro-collapse occurred (as evidenced by SEM images at the end of the cycle). This work suggests a prospective application of impedance measurements in driving process efficiencies by operating the dryer at the highest achievable temperature (i.e. the collapse temperature) whilst avoiding macro-collapse.

Keywords

Freeze-drying; Lyophilization; Process analytical technology; Impedance spectroscopy; Primary drying; Product temperature; Dry layer resistance; Sublimation rate; Micro-collapse; Glass transition temperature; Collapse temperature; Lactose

Nomenclature

A_e	Projected external cross-sectional area of the base of the vial (m^2)
A_i	Internal cross-sectional area of the vial (m^2)
A_s	Interfacial area between the TVIS electrode and the glass wall (m^2)
$\mathbf{C}$	Complex capacitance (F)
C_g'	Maximum freeze concentration (% w/w)
C''_{PEAK}	Peak amplitude of the imaginary part capacitance (dielectric loss) spectrum (F)
$\hat{C}''_{PEAK}$	Temperature compensated peak amplitude (F)
$\hat{C}''_{PEAK}(0)$	Temperature compensated peak amplitude (F) at the time point when the vacuum is applied
$C''_{PEAK}(T)$	Peak amplitude (F) at any temperature T
$C''_{PEAK}(t)$	Peak amplitude (F) at any time t
$\hat{C}''_{PEAK}(t)$	Temperature compensated peak amplitude (F) at any time t
$C''_{PEAK}(T_{ref})$	Peak amplitude (F) at the reference temperature T_{ref}
C_s	Capacitance of the TVIS vial and its content (F)
d	Ice layer thickness (m)
d_s	Average distance between the TVIS electrode pair, including the glass wall thickness (m)
$d\hat{C}''_{PEAK}/dt$	Surrogate measurement of the sublimation rate ($F \cdot h^{-1}$)
$dm_{\hat{C}''_{PEAK}}/dt$	Sublimation rate ($g \cdot h^{-1}$) derived from TVIS parameters $\hat{C}''_{PEAK}$
dm/dt	Sublimation rate ($g \cdot h^{-1}$)
dq/dt	Heat transfer (W or $J \cdot s^{-1}$)
$\boldsymbol{\varepsilon}$	Complex dielectric permittivity (dimensionless)
ε_o	Permittivity of free space (8.854×10^{-12} $F \cdot m^{-1}$)
ε_r	Relative permittivity (dimensionless)
f	Frequency (Hz)
F_{PEAK}	Peak frequency of the imaginary part capacitance (dielectric loss) spectrum (Hz)
h_{RE}	Height of liquid or ice layer within the electrode bounded region (m)
$h_{\hat{C}''_{PEAK}}(t)$	Height of ice layer within the electrode bounded region derived from TVIS parameters $\hat{C}''_{PEAK}$ (m) at any time t
h_{BE}	Height of ice layer below the electrode bounded region (m)
h_i	Predicted height of the ice interface (m)
$h_i(t)$	Predicted height of the ice interface (m) at any time t
h_n	Predicted height of TVIS node from the internal base of the vial (m)
$h_n(t)$	Predicted height of TVIS node from the internal base of the vial (m) at any time t
$h_{RE}(0)$	Height of ice layer within the electrode bounded region (m) at the time point when the vacuum is applied
$h_{RE}(t)$	Height of ice layer within the electrode bounded region (m) at any time t
h_t	Height of liquid or ice layer from the internal base of the vial (m)
k_i	Thermal conductivity of ice ($W \cdot m^{-1} \cdot K^{-1}$)
k_s	Cell constant of TVIS vial and its content (m)

l_d	Dry layer thickness (m)
$l_d(t)$	Dry layer thickness (m) at any time t
L_i	Latent heat of ice sublimation (W·s·g^{-1})
$m_{\hat{C}''_{PEAK}}(t)$	Ice mass within the electrode bounded region derived from TVIS parameters $\hat{C}''_{PEAK}$ (g) at any time t
m_{BE}	Mass below the electrode bounded region (g)
m_{RE}	Mass within the electrode bounded region (g)
$m_{RE}(0)$	Mass within the electrode bounded region (g) at the time point when the vacuum is applied
$m_{RE}(t)$	Mass within the electrode bounded region (g) at any time t
m_t	Total sample mass contained in the vial (g)
$m_t(t)$	Total ice mass contained in the vial (g) at any time t
m_{TE}	Mass when filled to the upper edge of the electrode (g)
ΔP	Pressure differential across the dry layer (bar or Pa)
P_c	Ice vapour pressure inside the freeze dryer chamber (bar or Pa)
P_{cd}	Ice vapour pressure at the condenser (bar or Pa)
P_i	Ice vapour pressure at the ice interface (bar or Pa)
P_v	Ice vapour pressure within the head space of the vial (bar or Pa)
$\emptyset$	Fill factor (dimensionless)
Φ	Temperature compensation factor for C''_{PEAK}
$\hat{R}_\rho$	Area-normalized dry layer resistance (Pa·m^2·s·g^{-1})
R_p	Product dry layer resistance (Pa·s·g^{-1})
R_s	Stopper resistance (Pa·s·g^{-1})
ρ_p	Resistivity of the dry layer (Pa·m^3·s·g^{-1})
$T_{F_{PEAK}}$	TVIS predicted temperature at the sensing node (°C)
T_b	Ice temperature at the internal base of the vial (°C)
T_c	Collapse temperature (°C)
T_{cd}	Ice temperature at the condenser (°C)
T'_g	Glass transition temperature of the maximally freeze-concentrated solution (°C)
T_i	Ice temperature at the sublimation interface (°C)
T_{ref}	Product temperature at the point at which the vacuum is applied to initiate primary drying (°C)
T_s	Shelf temperature (°C)
T_{TC}	Product temperature from the in-vial thermocouple (°C)
τ	Relaxation time (s)

Definition of TVIS terminology

Electrode bounded region	Refers to that part of the cylinder that is confined within the perimeter of the electrode pair which is occupied by ice. The cylinder can be thought of comprising concentric cylinders of the ice mass and the glass wall. This region does not include that part of the cylinder that is confined within the perimeter of the electrode pair which does not contain ice (i.e. the air space and the dry layer of the product are not included in this region)
TVIS node	That point at the center of the volume of frozen mass inside the vial which is bounded by the electrodes on the outside of the vial. Its position, in the vertical direction, is exactly half way up the ice mass that occupies the region bounded by the electrodes. In order to estimate its position from the inside base of the vial then the distance between the bottom of the electrode and the inside surface at the base of the vial is added to the half-height of the ice mass.
$Log\ F_{PEAK}$ calibration	A calibration plot of temperature vs $Log\ F_{PEAK}$ that is established during a temperature ramp which is incorporated into the lyophilization cycle after the freezing stage but before the onset of primary drying. The relationship between temperature and $Log\ F_{PEAK}$ over the sub-zero temperature range is modelled by a second order polynomial and the polynomial coefficients are used to estimate the temperature at the TVIS node from the values of $Log\ F_{PEAK}$ recorded during primary drying.
$T_{F_{PEAK}}$	Ice temperature, at the loci of the TVIS node, during the primary drying stage. These temperatures are predicted from a calibration of temperature against $Log\ F_{PEAK}$ which is recorded during a thermal cycle introduced into the lyo cycle before the initiation of primary drying. The assumption is that this temperature represents the average temperature of the ice in the region bounded by the electrodes [1].

Introduction

An increase in the number of approved lyophilization products over the last few decades continues to demonstrate that freeze-drying remains one of the most effective ways to achieve an acceptable product quality and shelf-life stability of injectable pharmaceuticals [2]. However, freeze-drying is a time consuming and costly process, factors that are driving the need for technological solutions which optimize product critical quality attributes (CQAs) while increasing the efficiency of the lyophilization process (in terms of increased batch uniformity and a reduction in drying times).

Of the three stages in the freeze-drying process, the primary drying stage is the longest and most energy-intensive. This is largely due to a requirement to dry at a sub-zero temperature, which is below either the glass transition of an amorphous product or the eutectic temperature of a crystalline product, in order to maintain the structure of the porous dry layer that results from sublimation of the ice. For the amorphous product, an increase in product temperature above the glass transition temperature of the freeze-concentrated solution (T_g') results in a progressive reduction in the viscosity of the dry layer. Once the viscosity of the solid-like state drops below 10^{12} Pa·s, which is the onset of substantial changes in material characteristics such as the dielectric relaxation time [3] then surface tension causes individual pores to merge into larger pores, the dry layer softens thereby reducing the mechanical strength of the cake and ultimately the dry layer collapses onto the ice that remains below. The temperature at which this occurs is the *collapse temperature* (T_c) or simply the *critical temperature*. Any excursion above this temperature alters the course of the rest of the drying cycle; slowing the rate of secondary drying (resulting in a higher final moisture content) while affecting other quality attributes such as the appearance and reconstitution time (with the possible rejection of the entire batch). Based on this understanding, attempts to improve the efficiency of the process by increasing the product temperature, whereby an 1 °C increase in product temperature can result in a ~ 13% reduction in primary drying time [4] is generally constrained by having to operate the dryer under conditions that avoid product collapse. Therefore, in order to design an effective and efficient lyo cycle, it is imperative to have an understanding of the temperature at which collapse is likely to

occur and to then design the cycle so that the product temperature remains below that critical threshold. For a number of years now, it has been standard industrial practice to predict the product collapse temperature for a freeze-drying process by an off-line technique known as freeze-drying microscopy (FDM). Typically, the collapse temperatures determined by FDM are 1-3 °C higher than the glass transition temperatures though in some cases this difference has been shown to be as high as 10 °C [5-7]. The premise for the in-process prediction of collapse (using FDM) is the assumption that the processes leading to collapse within the microscope are the same as those within the product container, i.e. glass vial. However, while FDM provides the conditions corresponding to the basic attributes of the first stages of the freeze-drying process (i.e. freezing followed by drying of the frozen sample at reduced pressure) the measurement is based on the microscale (i.e. 1-2 µL of sample) and therefore FDM results might not represent the bulk sample contained within a vial. This issue was realised when the collapse temperature measured by FDM was found to be ~ 3 °C lower than that measured in-vial by optical coherence tomography based FDM (OCT-FDM) [8,9]. However, one drawback of the OCT approach is that the bulky instrumentation associated with this technique does not lend itself to integration within a conventional freeze-dryer, without alteration to the hexagonal packing of the vials. It is therefore not clear whether the isolated vial presents the same product collapse potential as a vial within a cluster inside a conventional freeze-dryer. More recently, an optical fiber system (OFS) based on fiber Bragg grating (FBG) technology has been introduced for measuring the critical temperature during the freeze-drying cycle [10,11]. However, like all temperature probes, the insertion of the sensor within the product can alter the way in which the ice forms, which might in turn impact the properties of the unfrozen fraction and in particular its architectural microstructure and mechanical strength.

Another recently introduced technology for monitoring the freeze-drying process, through-vial impedance spectroscopy (TVIS) was shown by our research group to be sensitive to the collapse of a 3% w/v solution of sucrose. This technique measures the impedance spectrum of the solution in a standard glass vial, which has been modified with a pair of copper electrodes (of dimensions 5 mm

high by 19 mm wide) each with its own guard electrode, attached to the external surface of the vial [12]. The advantage over other single vial measurement techniques (including the use of temperature probes such as thermocouples) is that the electrodes are on the outside of the vial, and of low thermal mass, such that they do not interfere with the heat transfer mechanisms nor impact the nucleation and ice growth patterns within the vial. In that study the event that marked the onset of collapse was the dramatic change in the derivative of the imaginary part capacitance (dielectric loss) at 1 kHz. However, at that time we had a limited understanding of how to use TVIS for the measurement of other process parameters such as product temperature and sublimation rate.

We have explored those issues associated with the macro-collapse of the product[1] in terms of the impact on the progression of the cycle and the quality attributes of the product. However, there is some potential for a dramatic increase in primary drying rate if the product temperature is controlled between the glass transition temperature T_g' and the collapse temperature T_c. Between these temperatures, a partial collapse of the product known as *micro-collapse* [13] opens up the pore structure and reduces the resistance to vapour flux. Under these conditions, it is the combination of the higher product temperature and the lower resistance to vapour flow that result in faster sublimation rates and shorter drying times [14].

In this study, and using the example of a 5% w/v solution of lactose, we return to the application of TVIS in order to characterize the micro-collapse phenomenon, and develop methods for the determination of various critical process parameters: Ice interface temperature (T_i) and sublimation rate ($dm_{\hat{C}''_{PEAK}}/dt$); from which the dry layer resistance is then determined.

Unlike the previous studies [1,12,15-18] here we use an alternative design of the TVIS measurement vial, i.e. one with a pair of electrodes each of dimension 10 mm high and 19 mm wide, but without the guard. The primary reason for this change to the electrode geometry is that we could use the rate of change in the amplitude of the ice relaxation peak (from the beginning of sublimation)

[1] i.e. when the dry layer has entirely collapsed leaving no remnant of the porous structure that once defined the dry layer

as the basis for our recent method [19] for determining the sublimation rate. In the previous collapse study with 5 mm high electrodes [12] the height of the frozen layer was above the top of the electrode at the beginning of the sublimation phase and therefore it was not possible to record the initial rate of drying.

1. Materials and Methods

1.1 Preparation

D-lactose monohydrate was purchased from Sigma® Life Science (UK) and used, as supplied, in the preparation of a 5% w/v lactose solution in ultrapure water (18.2 MΩ·cm).

1.2 Differential scanning calorimetry

The glass transition (T_g') of the freeze-concentrated 5% w/v lactose solution was analyzed by modulated differential scanning calorimetry (mDSC) using a Q2000 DSC, TA instrument (UK) according to the following method. A 80 µl sample of 5% w/v lactose solution was placed in a sealed aluminium pan (part number 900825.902) and cooled down to −90 °C at a 10 °C·min^{-1} and then re-heated to 25 °C at 1.5 °C·min^{-1}, with a modulation of 0.23 °C·min^{-1} every 60 s. Nitrogen was purged during measuring at a flow rate of 50 mL·min^{-1}. The temperature at the midpoint of the thermal transition was obtained by Universal Analysis 2000 software (TA Instruments, New Castle, USA) and used to define the glass transition temperature of the maximally concentrated solution (T_g').

1.3 Freeze-Drying Microscopy

The collapse temperature (T_c) of the dry layer, resulting from the freeze-drying of the 5% w/v lactose solution, was determined using a Lyostat5 freeze-drying microscope (FDM) from Biopharma Process Systems (UK) according to the following method. A 2 µl sample of the 5% w/v lactose solution was pipetted onto a 16 mm circular quartz window located on a silver block of the FDM stage, and then covered with a glass coverslip (13 mm diameter) supported by a 70 µm spacer. A small amount of silicon oil was used to improve the thermal transfer from the silver block to the quartz window. The sample was then cooled to −50 °C, at a rate of 10 °C·min^{-1}, and held for 2 min to ensure complete solidification, before the vacuum was applied (pressure < 0.02 mbar) in order to initiate sublimative drying. Once a sufficient dry layer depth had developed, the sample was then heated to 20 °C, initially at a rate of 5 °C·min^{-1} then at a slower rate of 1 °C·min^{-1} when temperature reached −35 °C, so as to be able to more accurately determine the onset of collapse temperature. Images were recorded every 5 s when the heating temperature was above −35 °C.

1.4 Vial filling and loading the freeze dryer

3.1 g aliquots of the 5% w/v lactose solution were transferred to a cluster of eighteen 10 mL type I tubular clear glass vial (1096936, Schott, Hungary supplied as VC010-20C from Adelphi - HP) and to one TVIS measurement vial. The fill weight of 3.1 g is equivalent to a liquid fill height of 9 mm from the internal base of vial, which corresponds to a fill factor (Ø) of 0.7, where Ø is defined as the relative height of sample solution within electrode region to the height of the electrode (as demonstrated in Figure 1). The TVIS vial was the same type of tubular glass vial but modified by attaching a pair of copper foil electrodes to the external surface of the vial. These two electrodes, each of height 10 mm and width 19 mm, are placed diametrically opposite one another and at a height of 3 mm above from the exterior base of vial.

It has been shown that TVIS measures the average product temperature at the center point of the volume of material bounded by the electrodes [1]. In other words, at a height which is equivalent to the half of the sample height bounded by electrodes; the point that we shall now call the TVIS temperature sensing node or simply the TVIS node (See Figure 1).

Two T-type thermocouples (28 AWG) were inserted into one of the vials, through the rubber stopper, and the tips positioned at the two specific heights; one at the center bottom of vial (TC2) and the other (TC1) at the equivalent height to the sensing node in the neighboring TVIS vial, as shown in **Error! Reference source not found.**. The positions of the TCs beads were realized through careful manipulation of the wires via a process of trial and error, with the final position being determined by eye. The TC containing vial was then placed adjacent to the TVIS vial.

Assuming that there is thermal equivalence between the two points in the horizontal direction of each of the adjacent vials then it follows that TC1 data from the annealing stage could be used to provide a calibration temperature for the TVIS vial (Section 2.4.1). This calibration then serves the purpose of providing a predictive temperature in the TVIS vial during the subsequent primary drying stage (Section 2.4.2). The second thermocouple (TC2) measures the product temperature at the base of the TC vial. Again, if one assumes thermal equivalence between the two points, one at the base of

the TC vial and the other at the base of the TVIS vial, then one can estimate the temperature at the sublimation front (T_i) using the 2-point linear extrapolation as the method published by Smith et al. [19] with the TVIS predicted temperature ($T_{F_{PEAK}}$) at the sensing node as the second point from which the extrapolation is projected

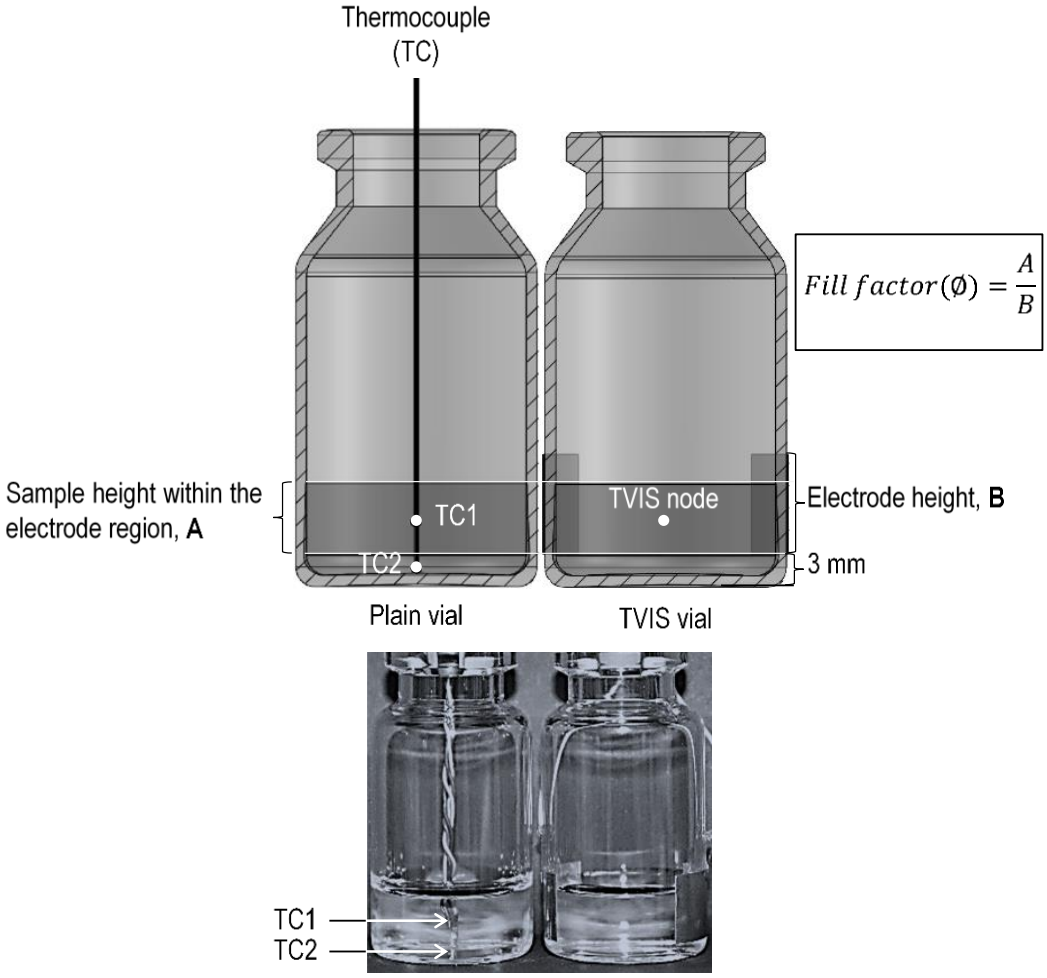

Figure 1 Vertical cross sections of two vials containing 3.1 g of 5% w/v lactose solution. Right: Modified TVIS vial attached with a pair of copper electrode (10 x 19 mm) positioned at 3 mm from the external vial base (~ 2 mm from the internal base of vial). Left: Unmodified "nearest neighbor" vial with two type-T thermocouples. The beads of the thermocouples were placed at the bottom center of the vial (TC2) and at the height which corresponds to the middle of sample within electrode sensing region (TC1). The fill factor (Ø) shown here is 0.7, which means that the sample height in the electrode region is 7 mm for an electrode height of 10 mm.

One hundred and sixty vials were arranged on the loading tray of the freeze-dryer, with the cluster of the 19 solution-filled vials at the centre of an array of empty vials (as shown in Figure 2) and then partially closed with 20 mm 4023/50 bromobutyl grey rubber stoppers (FDW20RTS, West

Pharmaceutical Services Singapore Pte. Ltd, Singapore) before loading into a VirTis Advantage Plus XL benchtop freeze dryer (SP Scientific, USA).

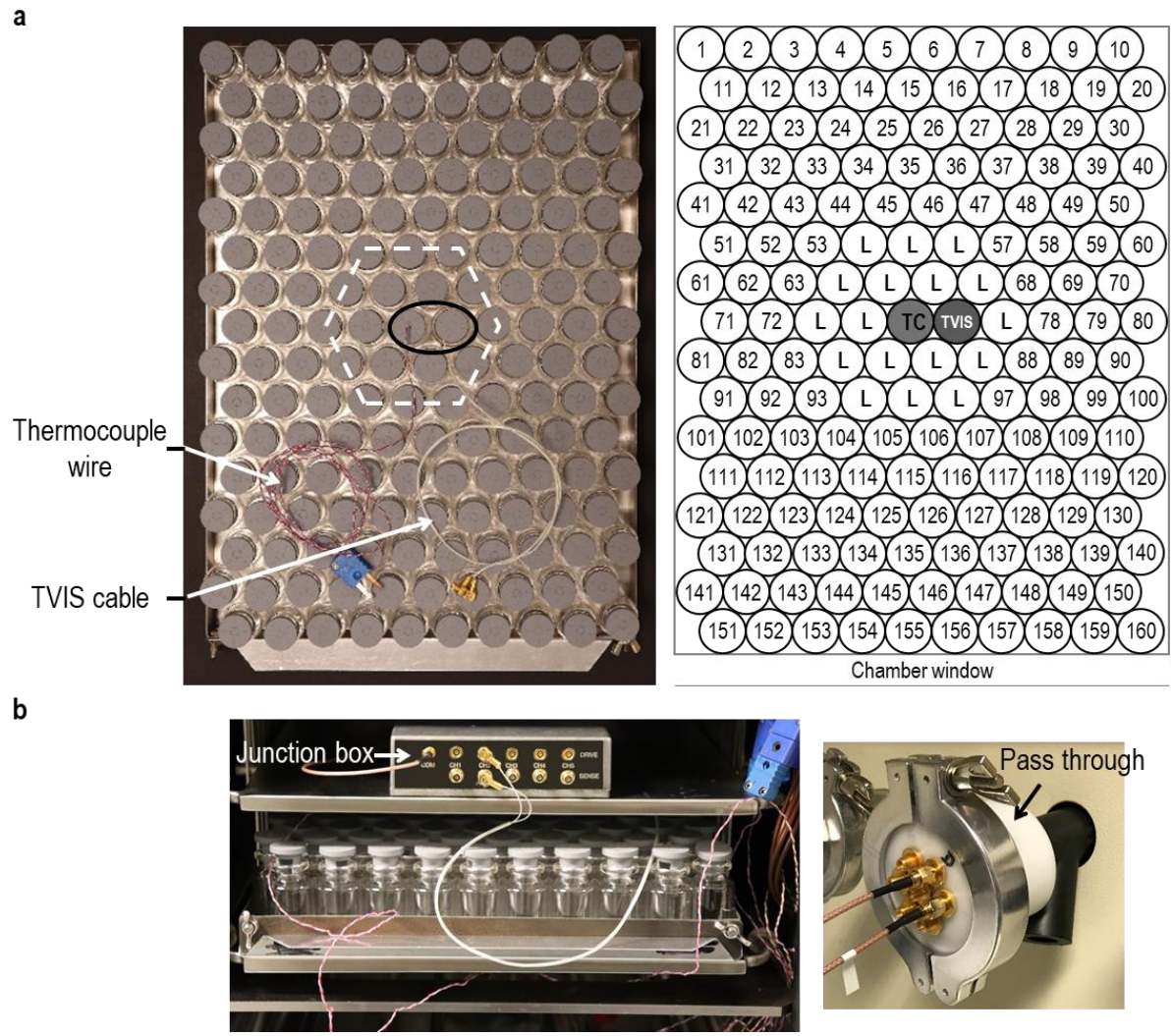

Figure 2 (a) Arrangement of vials on the shelf of the VirTis Advantage Plus XL freeze-dryer. The TVIS modified vial (labelled TVIS) and the thermocouple containing vial (labelled TC) were placed close to the centre of the shelf. The sample filled vials are represented by "L" and those left empty are labelled with the number position in the dryer. (b) Five channels TVIS junction box (left photo) placed on freeze-dryer shelf, and the pass-through (right photo) for the TVIS cabling which is connected to the manifold hose on the outside of a Virtis Advantage Plus XL freeze-dryer.

1.5 Through vial impedance spectroscopy (TVIS)

The TVIS measurement vial was connected to a multichannel impedance analyzer developed by De Montfort University via a junction box inside the freeze dryer (Figure 2b) and an electrical pass-through on one of the manifolds on the dryer (Figure 2b). A full description of the measurement system is given by Smith and Polygalov [20].

Impedance spectra of the TVIS vial, over the frequency range of 10 Hz to 1 MHz, were measured throughout the entire freeze-drying process at a scan interval of 2 min. The measurement time to acquire each spectrum was ~ 10 s

1.6 Freeze drying protocol

The process cycle described in Table 1 was used to freeze dry the 5% w/v lactose solution. Three specific features were included in this cycle (see those items in bold in Table 1):

Table 1 Freeze-drying protocol.

Step	Temperature (°C)	Time (min)	Cumulative Time (h)	Set pressure (µbar)
Equilibrium phase	+20	10	0.17	-
Freezing temperature ramp (0.6 °C·min^{-1})	−50	120	2.17	-
Freezing temperature hold	−50	120	4.17	-
Re-heating temperature ramp (0.7 °C·min^{-1})	−10	60	5.17	-
Re-heating temperature hold	−10	120	7.17	-
Re-cooling temperature ramp (0.7 °C·min^{-1})	−50	60	8.17	-
Re-cooling temperature hold	−50	120	10.17	-
Primary drying temperature ramp (0.3 °C·min^{-1})	−40	30	10.67	-
Primary drying temperature hold	−40	30	11.17	-
Primary drying temperature hold	−40	60	12.17	**300**
Primary drying temperature ramp (0.1 °C·min^{-1})	−10	300	17.17	**300**
Primary drying temperature hold	−10	1560	43.17	**300**

(i) A re-heating stage between −50 °C and −10 °C (after the freezing hold period) in order to calibrate the TVIS peak frequency (F_{PEAK}) against product temperature and to establish the correction coefficient to compensate for the impact of temperature on the TVIS parameter, C''_{PEAK}, so that product temperatures and sublimation rates may be predicted in the subsequent primary drying stage.

(ii) A ramp in the shelf temperature during the primary drying step from −40 to −10 °C in an attempt to force the product through its glass transtion and thereby collapse the product.

(iii) A partial vacuum of ~ 290 µbar (0.029 kPa) during the primary drying stage was aimed to create an initial sublimation interface temperature of −32 °C (which corresponded to be the onset of the glass transition measured by mDSC).

1.7 Scanning electron microscope (SEM)

The microstructure of the freeze-dried cake (following extraction from the TVIS vial) was examined by a scanning electron microscope (Carl Zeiss EVO HD, UK). To this end a vertical cross-section of the lactose cake was mounted on an aluminum stub using Electrodag® 1415 (Agar Scientific) coating as an adhesive, and then sputtered with gold under vacuum, using Quorum Q150RS sputtering coater, to a thickness of 15 nm. Images showing the morphology of the freeze-dried cake were acquired at 25x magnification, for an overview of the whole sample, and at 500x magnification for a more detailed view of the microstructure at different depths of freeze-dried cake (i.e. top, middle and bottom sections).

2. Results and Discussions

2.1 Glass transition temperature of the freeze concentrate (T'_g) by mDSC and the collapse temperature (T_c) by FDM

An endothermic step in the reverse heat flow diagram of the mDSC thermogram was used to demonstrate the glass transition behaviour of the 5% w/v lactose solution. There are several methods for assigning a temperature to the glass transition; however, the mid-point of the step is possibly the most common [21]. According to this method we derived a value of T'_g = −30.2 °C for the 5% w/v lactose solution (as shown in Figure 3). This temperature agrees broadly with the midpoint T'_g values ranging from −27 and −33 °C in other works [22-24].

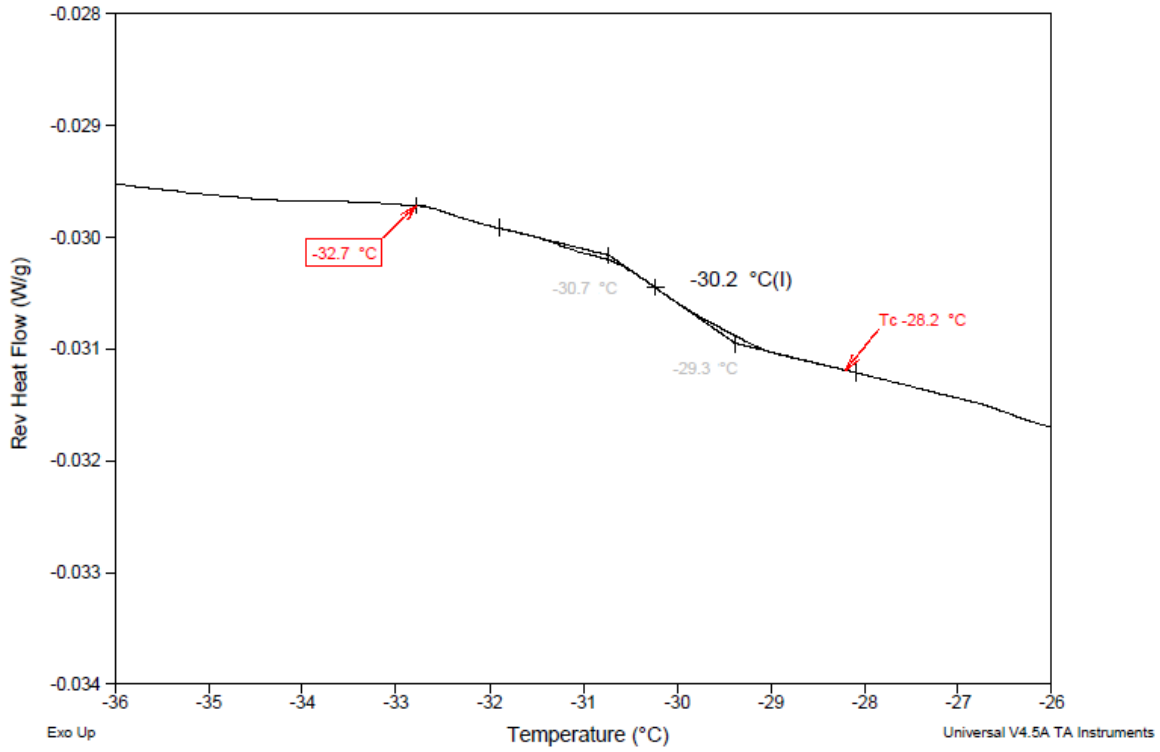

Figure 3 A mDSC thermogram of 5% w/v lactose solution. The glass transition temperature of the maximally freeze concentrated solution (T'_g) of −30.2 °C is demonstrated by a step in a reverse heat flow.

The onset of the collapse of the 5% w/v lactose solution was recorded at T_c = −28.2 °C (Figure 4b) which is ~ 2 °C higher than our value for T'_g taken from the midpoint of the reverse heat flow thermogram. It is assumed that the higher the temperature difference between both critical formulation parameters (i.e. T'_g and T_c) the higher the upper tolerance limit for driving the efficieny of the process whilst avoiding collapse.

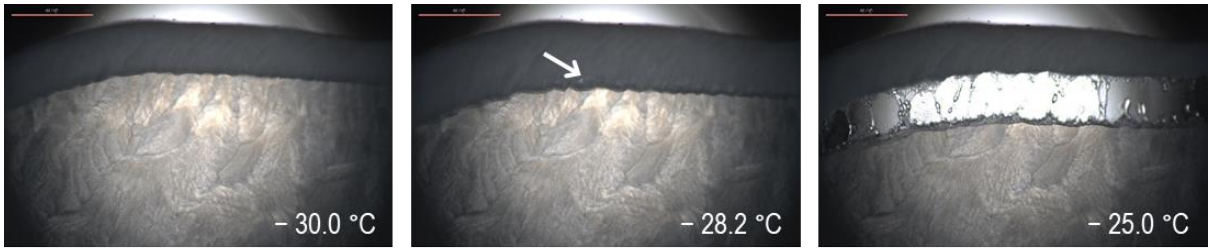

Figure 4 An example of freeze-drying microscopy images of 5% w/v lactose solution. (a) drying at −30.0 °C, (b) onset of collapse at −28.2 °C, and (c) complete collapse at −25 °C.

2.2 Process parameters

Figure 5 shows the freeze-drying profile of the standard process parameters: the shelf temperature (T_s), the product temperature (T_{TC}) from the two thermocouples, and the chamber pressure (P_c). The product temperature (T_{TC}) provided evidence for: (i) a nucleation temperature of −12.4 °C in the TC containing vial with an uncertainty estimate of 0.4 °C, determined from half the difference between the two temperatures recorded by TC1 and TC2 in the nearest neighbour vials, (ii) the thermal equilibration of the product with the shelf being reached within each of the 2 h hold periods after the freezing stage, the annealing hold stage, and the end of the re-cooling phase of the annealing cycle. The thermocouple probe also evidenced the increase in product temperature during the shelf temperature ramp of the primary drying stage, with the slowing rate of increase in the product temperature being associated with the onset of drying (due to the phenomenon of self-cooling). At 18 h the system enters the steady state period with a constant product temperature, once the shelf temperature reached its set value of −10 °C at 18 h. The onset of a step-like increase in the thermocouple temperature at 19.9 and 20.4 h (for TC1 and TC2, respectively) is probably an artefact induced by the bead of the TC detaching (i.e. losing contact) with the ice layer, as discussed later in this article.

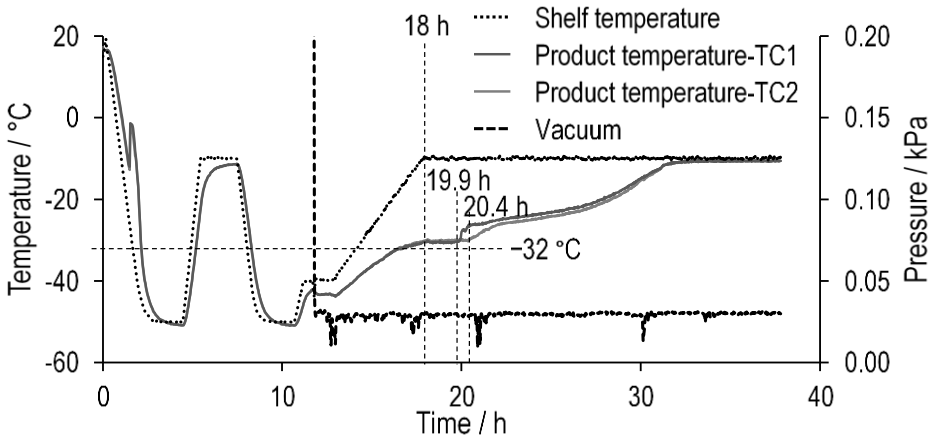

Figure 5 Freeze drying process profile of 5% w/v lactose solution.

2.3 TVIS results

Figure 6 shows the surface plot of the real and imaginary capacitances of the TVIS vial, filled with 3.1 g of a 5% w/v lactose solution, throughout the entire lyophilization cycle. Each plot is made up from the multiple individual spectra that were acquired every 2 min throughout the cycle. The real part capacitance defines the ability of a material to store the electrical potential energy through an alignment of localized charges associated primarily with polar molecules, whereas the imaginary part capacitance defines the ability of a material to dissipate energy through either the diffusion of delocalized charges associated with ions (in the case of conductivity) or the lag between the oscillations of applied electric field and the response of the polarization processes (in the case of dielectric loss), for example.

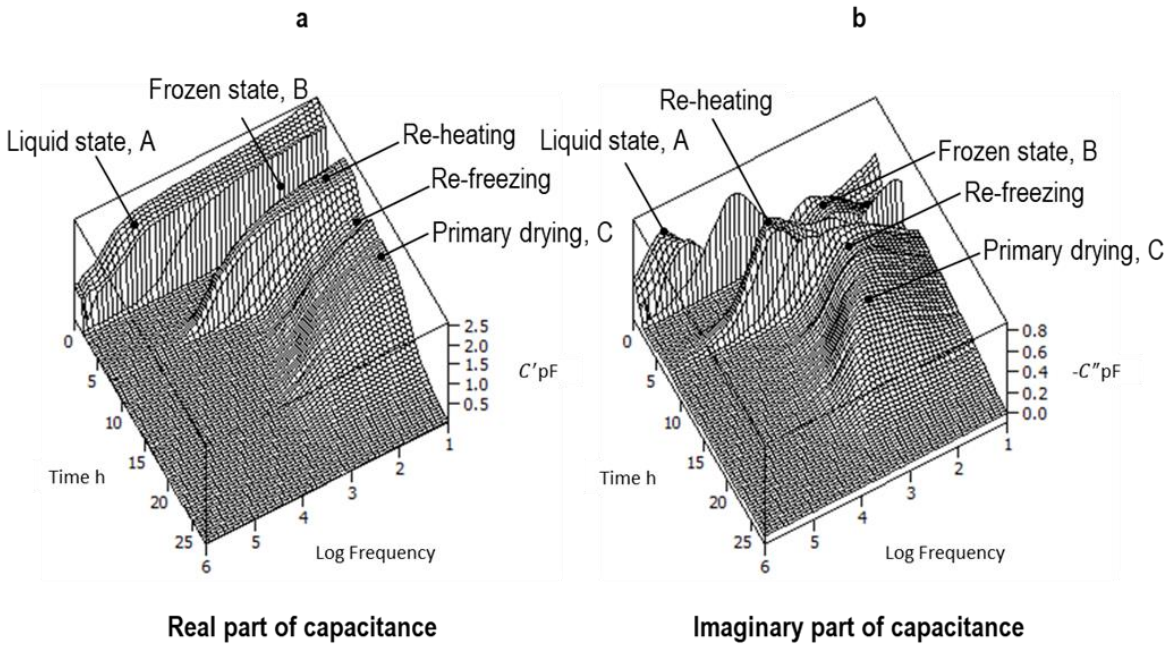

Figure 6 (a) Real and (b) imaginary capacitance spectra recorded every 2 min during the freeze-drying of the 5% w/v lactose solution.

In order to provide a clearer picture and commentary on the changes observed during the lyo cycle we have taken example spectra for each phase of the cycle and then plotted in Figure 7. Prior to ice nucleation and growth (Phase A in Figure 6) the step in the real part capacitance spectra and the main peak in the imaginary capacitance spectra is due to the Maxwell-Wagner (interfacial) polarization of the glass wall through the solution resistance. After complete solidification of the ice mass (Phase B in Figure 6) then the polarization mechanism changes and the process is associated with the dielectric relaxation of ice; the time constant of which has a temperature dependence that has been studied on numerous previous occasions and reported in key texts by Johari and Whalley [25] and Popov et al. [26]. As the process enters primary drying (Phase C in Figure 6) then the magnitude of the dielectric loss process reduces as ice starts to sublime. Smith and Polygalov [20] gave descriptions of the mechanisms underpinning the Maxwell-Wagner process and the dielectric relaxation of ice.

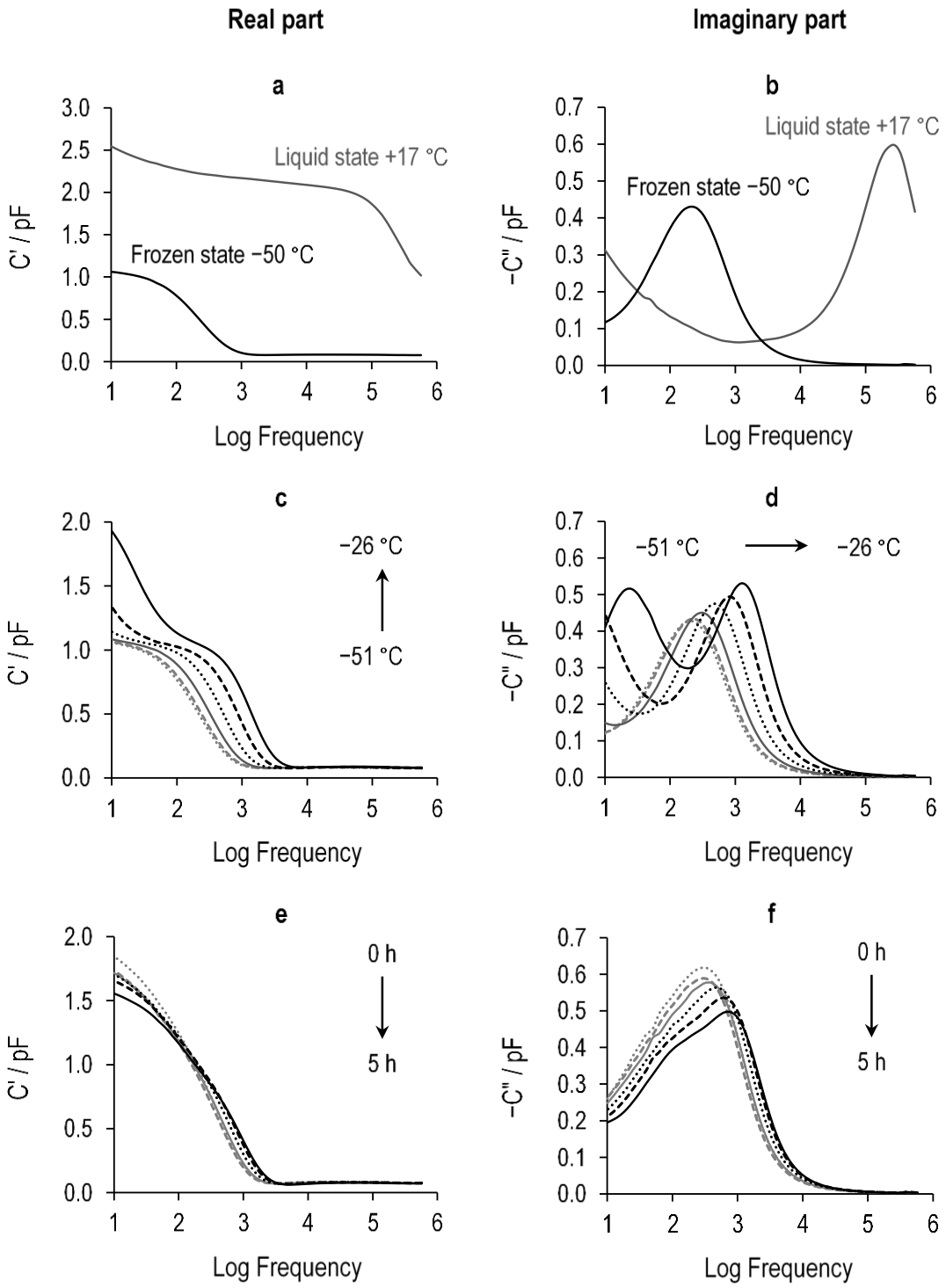

Figure 7 An example TVIS spectra of 5% w/v lactose solution during (a-b) freezing, (c-d) re-heating from −51 °C to −26 °C and (e-f) primary drying (0-5 h)

Here, we note the differences between our study and those dielectric studies of Johari and Whalley [25] and Popov et al. [26]. In those published studies, water is frozen and measured inside a parallel plate capacitor with direct contact between the metal electrodes and the sample; whereas in our study, we have an additional impedance in series with the sample (owing to the juxtaposition of

the glass wall with the sample) which shifts the characteristic frequency and amplitude of the dielectric loss peak relative to that due to the relaxation process of ice alone. The impact of the glass wall impedance on the experimentally measured relaxation process is the subject of preliminary analysis by Smith and Polygalov [20]. We also note that the co-existence of the unfrozen fraction also affects the experimentally observed spectrum by introducing a second process at lower frequencies than the main dielectric relaxation of ice. The analysis of the impact of the glass wall impedance on the measured spectra is out of the scope of this publication. Instead, we resort to a more empirical approach based on the peak amplitude and peak frequency of the dielectric loss process associated with the dielectric relaxation of the ice fraction. Note therefore, that the peak frequency cannot be used directly to calculate the relaxation time (τ) according to the standard formula, $\tau = 1/2\pi f$, where f is frequency. Nor can one calculate the complex dielectric permittivity ($\boldsymbol{\varepsilon}$) of the ice fraction from the complex capacitance ($\mathbf{C}$) according to the standard formula, $\boldsymbol{\varepsilon} = \mathbf{C}/\varepsilon_o k_s$, where ε_o is the permittivity of free space and k_s is the cell constant of the object (in our case the TVIS vial and its contents).

Also, the analysis of the freezing stage of simple sugar solutions (such as lactose and sucrose) will be the subject of another article and instead we focus exclusively on the annealing stage and the primary drying stage. The peak-finding function of our LyoView™ analytical software was used to determine the amplitude (C''_{PEAK}) and the characteristic frequency (F_{PEAK}) of the dielectric loss peak across the re-heating phase of the annealing stage and the primary drying stage from the starting to the point at which C''_{PEAK} had effectively reduced to zero. An example spectrum, which highlights the determination of C''_{PEAK} and F_{PEAK} and also the existence of a secondary relaxation peak associated with the unfrozen fraction is shown in Figure 8.

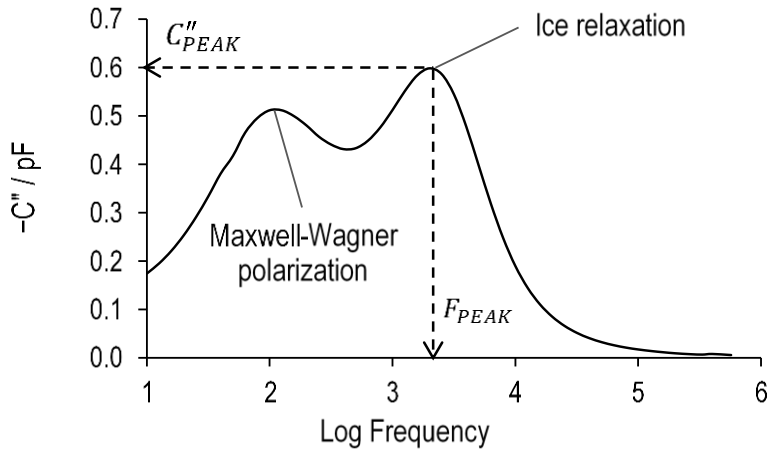

Figure 8 An example dielectric loss spectrum of the 5% w/v lactose solution at −20.3 °C (during re-heating of the frozen solution) to demonstrate the meaning of C''_{PEAK} and F_{PEAK} of the ice relaxation peak as determined by the LyoView™ software.

In our previous publication [19] we demonstrated the sensitivity and subsequent application of the TVIS parameter F_{PEAK} in the determination of the ice interface temperature during primary drying, and the sensitivity and subsequent application of the TVIS parameter C''_{PEAK} in the determination of the primary drying rate; from which an estimation of the vial heat transfer coefficient could be derived. In that work we used a dual-pair electrode system. Here, we further develop this approach and adapt the method for a single pair of electrodes. Figure 9 shows a schematic of the principles of this new method

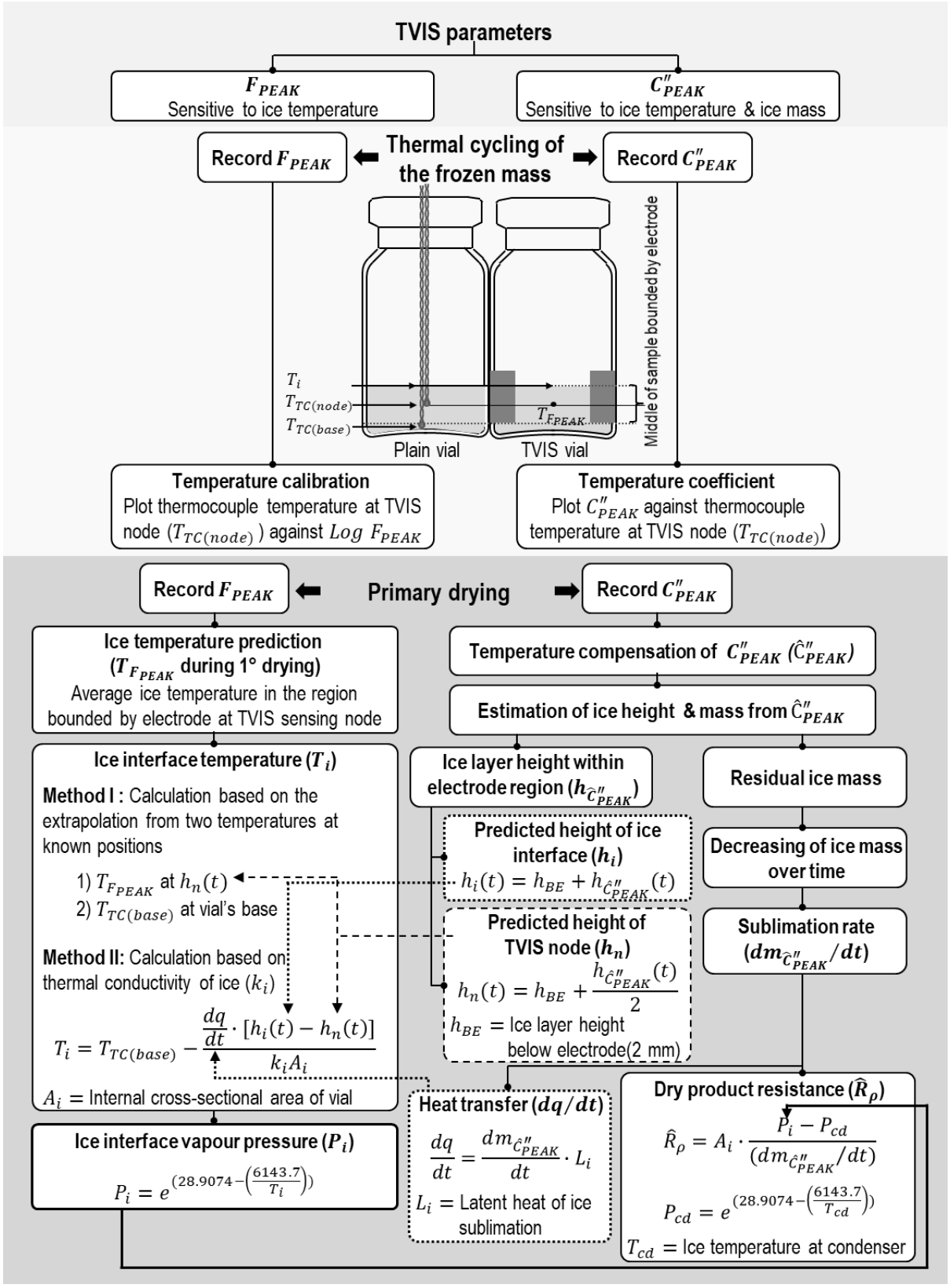

Figure 9 A schematic of the TVIS method for determining drying rate and ice interface temperature from which the dry layer resistance is estimated

2.4 Measurement of product temperature

2.4.1 Ice temperature calibration

Johari and Whalley [25] demonstrated that there is a positive correlation between the relaxation frequency of ice and its bulk temperature. It is not surpising therefore to find that the peak in the imaginary capacitance spectrum shifts to higher frequencies as the temperature of the frozen matrix within electrode region is increased (Figure 10a). Therefore, a temperature calibration could be provided using TVIS data from the re-heating phase of the annealing cycle by first plotting the temperature from the thermocouple located at TVIS node (T_{TC1}) in a nearest neighbor vial against the TVIS peak frequency on a logarithm scale ($Log\ F_{PEAK}$) for the corresponding times at which the temperature was recorded, and then fitting a second order polynomial function to the data (Figure 10b).

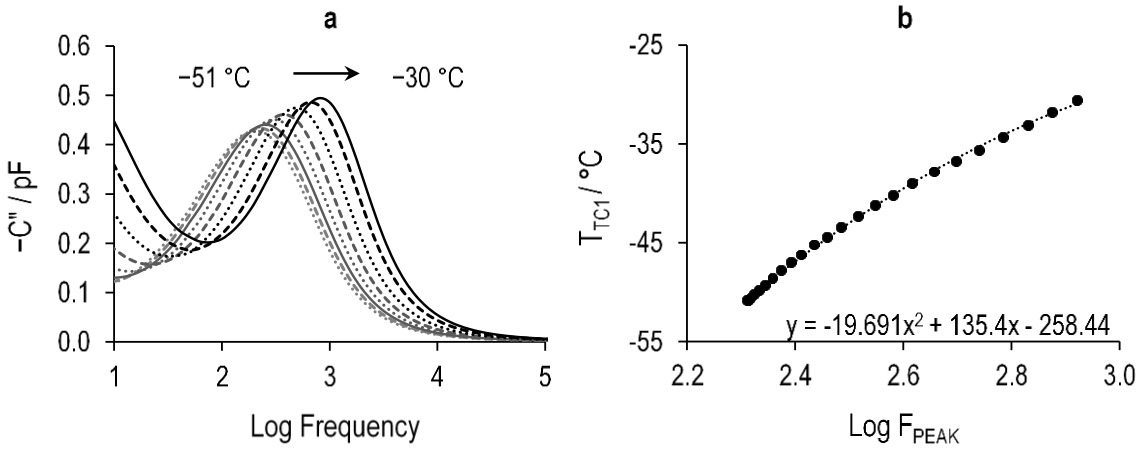

Figure 10 (a) Selected imaginary capacitance spectra of 5% w/v lactose solution in a 10 mL TVIS measurement vial with a pair of 10 x 19 mm electrodes, demonstrating the temperature dependency of the dielectric loss peak during the reheating stage (temperature ramp from −51 to −30 °C at 0.7 °C·min^{-1}); (b) Temperature calibration used for estimating the ice temperature during primary drying is determined from the plot of the thermocouple temperature located at the TVIS node, i.e. the mid-point of sample within electrode region (T_{TC1}) and the logarithm of the peak frequency (F_{PEAK}) as recorded during the reheating period.

2.4.2 Prediction of ice temperature at the TVIS node

The averaged product temperature of the ice in the region bounded by the electrodes, during the subsequent primary drying stage, is then predicted by substituing values for $Log\ F_{PEAK}$ (from the primary drying period) into the x-parameter of the polynomial function (shown in Figure 10b). Note that the predicted temperature at the TVIS node has the symbol $T_{F_{PEAK}}$ because it is derived from the

TVIS parameter F_{PEAK}. Figure 11 shows values for both the TVIS predicted temperature ($T_{F_{PEAK}}$) and the thermocouple measured temperature ($T_{TC1}$and T_{TC2}) along with the shelf temperature (T_s).

A few initial points are worth noting concerning Figure 11:

1. The temperature predicted by TVIS ($T_{F_{PEAK}}$) matched the profile from the temperature sensor ($T_{TC1}$and T_{TC2}) for the first 8.1 h of primary drying, with the maximum difference of 1.7 °C and a 0.5 °C difference on average, throughout that period.
2. Both $T_{F_{PEAK}}$ and thermocouple temperature ($T_{TC1}$and T_{TC2}) stabilise at a temperature of −30.6 ± 0.36 °C between 6.4 and 8.0 h (i.e. soon after the shelf temperature had entered the hold period at 6.2 h into primary drying).
3. At 8.1 h there is a pronounced step in the T_{TC1} profile resulting in T_{TC1} being on average ~ 5 °C higher than $T_{F_{PEAK}}$ over the subsequent period between 8.2 and 12.3 h.
4. After 10 h, both T_{TC1} and $T_{F_{PEAK}}$ increase graduallly even though the shelf temperature continued to remain constant.
5. The temperature profile from T_{TC2} demonstrates a similar phenomenon to that from T_{TC1} but the step appears at the later time point (8.6 h) and is much less dramatic in terms of the rate of increase in temperature. The temperature from T_{TC2} is ~1 °C lower than that from T_{TC1} on average after 10.4 h owing to its position closer to the colder sublimation interface.

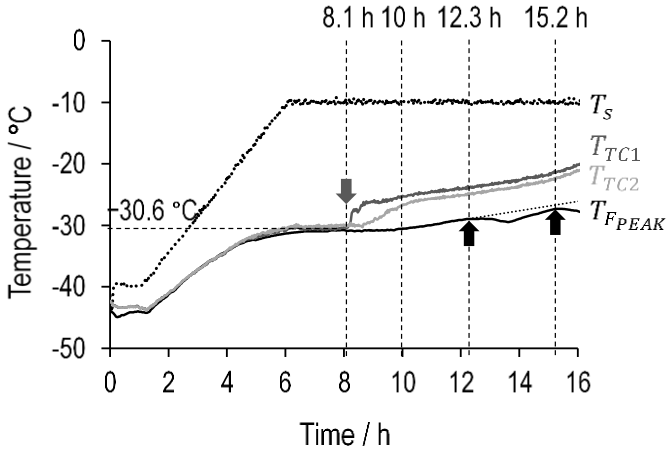

Figure 11 Temperature profiles during the primary drying stage, showing the thermocouple temperature (T_{TC}), the TVIS predicted temperature ($T_{F_{PEAK}}$), and the shelf temperature (T_s). The downward grey arrow marks the step in the T_{TC1} profile at 8.1 h whereas the two upward black arrows mark the dips in the $T_{F_{PEAK}}$ profile at 12.3 and 15.2 h, respectively. The dotted line extrapolated from $T_{F_{PEAK}}$ data (from the 12.3 h time point onwards) is drawn to show the expected response if it were to follow a trajectory which is similar to that displayed by the thermocouple temperature (T_{TC}).

As sublimation proceeds, a decrease in the quantity of ice could lead to the thermocouple sensor detaching from the ice thereby increasing the uncertainty in the measurement of the product temperature [27-29]. It is highly likely, therefore, that the step-like increase in the thermocouple temperature at 8.1 h is due to this phenomenon (see grey downward arrow on Figure 11). However, the TVIS predicted product temperature continues beyond 8.1 h along a constant trajectory, suggesting that TVIS might be able to track the product temperature over a longer period than the TC sensor. Possible explanation for the differences in the duration of the two temperature tracking periods is that the thermocouple probe was located at the center of sample bounded by sensing electrode, and so once the ice has been removed to that point then the thermocouple will begin to sense the temperature of the dry layer rather than the temperature of ice. In contrast, the TVIS system has the sensing electrodes outside of the vial and the temperature predicted by this technique represents the average temperature of that part of the product bounded by the electrodes.

Despite the systematic error of the TC sensor associated with the thermocouple profile (i.e. the step in the measured temperature) the measured temperature continues thereafter on a monotonic trajectory. In contrast, the $T_{F_{PEAK}}$ profile dips in two places, first at 12.3 h and then at 15.2 h (see black upward arrows on Figure 11). Our assumption is that the dips in the trajectory of $T_{F_{PEAK}}$ is symptomatic of the change in the ice cylinder contact with the inside of the glass vial. Notwithstanding both artefacts with the TC and TVIS measurements of temperature, it is interesting to note that the general profiles of both measurements beyond 10 h, again follow the same trend, which is a gradual increase in temperature related to a slow-down in primary drying rate and the associated reduction of the self-cooling of the contents. The dotted line on the $T_{F_{PEAK}}$ data beyond 12.3 h is drawn to indicate the trend if those two dips are not evident.

2.5 Estimation of the residual ice mass

By making an analogy between the TVIS vial (with the electrodes on the outside of a glass vial filled with a frozen solution) and a parallel plate capacitor, one can expect the electrical capacitance of the TVIS vial to be a function of the interfacial area of the frozen matrix that intimately contacts the

inside surface of the glass wall that is adjacent to the electrode. An approximation for this capacitance can therefore be taken from the basic equation for electrical capacitance of the parallel plate capacitor (Equation 1).

$$C_s = \frac{\varepsilon_o \varepsilon_r A_s}{d_s} \qquad \text{Equation 1}$$

For the parallel plate capacitor, C_s is the capacitance of the object (i.e. the TVIS vial and its contents), ε_o is the permittivity of free space (8.854 x 10^{-12} F·m^{-1}), ε_r is the relative permittivity of the composite sample (the frozen mass in series with the glass wall of the vial), A_s is the interfacial area between the TVIS electrode and the glass wall, and d_s is the average distance between the TVIS electrode pair including the glass wall thickness.

It follows that a decrease in the interfacial area, associated with the reduction in the height of the ice layer in contact with glass wall, would result in a proportional decrease in the capacitance of TVIS vial. In other words, the capacitance of the TVIS vial is directly porportional to the amount of ice contained in the vial. Consequently, the rate of ice loss could be determined by the rate of change of the measured capacitance, thereby providing an opportunity for monitoring the primary drying process. Smith et al. [1] descibed the basic methodology for the determination of sublimation rate by using the magnitude of dielectric loss process associated with the ice content in the vial (C''_{PEAK}).

It is thought that the linearity between the amplitude of the dielectric loss peak (i.e. C''_{PEAK}) and the height of the ice cyclinder is dependent on the intimacy of ice contact with the inside of the glass wall. Therefore it is not recommend to follow this parameter throughout the entire primary drying process (for the purpose of determining the primary drying rate) due to the inevitable changes in the ice-glass contact associated with a change in the shape of the ice cylinder towards the latter part of the drying process. We have suggsted previously [19] that the point at which this measurement uncertainty is realised could be predicted by a decrease in the magnitude of F_{PEAK} in circumstances when the actual product temperature continues to increase during drying. The identification of this time point then allows for any unreliable data to be excluded from further analysis. On this basis, we

consider that the ice cylinder begins to detach from the side wall at 12.3 h (again we refer you to the first of the two upward black arrows on Figure 11). However, the combination of factors associated with ice shape, uncertainty of TVIS measurement at points near the edges of electrode (i.e. fringing effect), and heat tranfer variation means that those process parameters determined from TVIS parameters, F_{PEAK} and C''_{PEAK}, are probably unreliable beyond 9 h and should therefore be disregarded from further consideration.

2.5.1 Compensation of C''_{PEAK} for temperature.

In our previous article documenting the use of TVIS in the determination of the heat transfer coefficient, we demonstrated a requirement to the first compensate C''_{PEAK} for its temperature dependency before correlating the parameter with a reduction in ice mass. Figure 12a shows the correlation between the peak magnitude and temperature during the temperature ramp-up of the annealing stage. The positive correlation with temperature is at first unexpected, given that the static permittivity of ice alone (i.e. without the series impedance of the glass wall) obeys the Curie-Weiss law, decreasing by ~ 17% from 130 at −73 °C to 108 at −33 °C [30]. However, recognizing that the measurement system includes an additional series impedance from the glass wall of the vial then one should also consider the impact of this capacitance on the amplitude and characteristic frequency of the relaxation peak. The impedance of this composite system (i.e. sample in series with glass wall) is further complicated by a double layer capacitance (at the interface between the frozen solution and the glass) which also contributes to the overall measured capacitance of the TVIS vial. This double layer is a function of the protonic and ionic charge accumulation at the surface of the glass from thermally activated diffusion processes in the ice and unfrozen fraction. It follows that the higher temperatures result in greater charge accumulation and therefore a higher interfacial capacitance and consequently a higher overall measured capacitance. This positive temperature coefficient must be larger than the negative temperature coefficient of the static permittivity of ice for the overall coefficient to be positive. It follows that C''_{PEAK} provides an indirect assessment of the microstructure of the frozen solid and suggests that the reduction in the amount of ice mass is not the only factor

defining the magnitude of C''_{PEAK}. It is possible, therefore, that without a correction for temperature then any change in the product temperature during primary drying could manifest as either a decrease in the apparent sublimation rate (in the case of the temperature increasing during primary drying) or an increase in the apparent sublimation rate (if the product temperature decreases during primary drying).

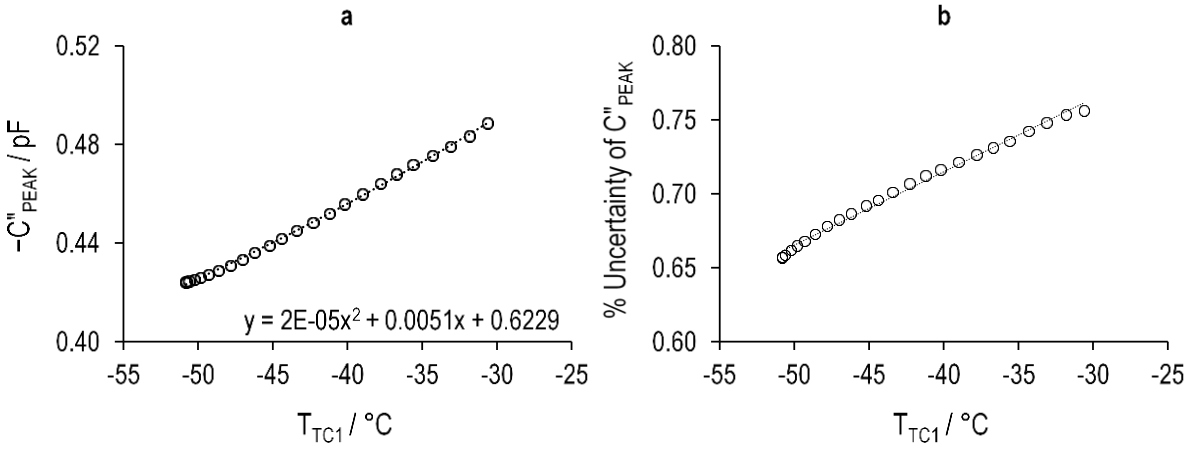

Figure 12 (a) Temperature coefficient of the peak amplitude (C''_{PEAK}) during re-heating from −51 to −30 °C at 0.7 °C·min^{-1}. (b) The first derivative of the temperature coefficient of C''_{PEAK}, divided by the value of C''_{PEAK} at the same temperature (expressed as a percentage) is referred to as the percent uncertainty, which is on average ~ 0.70% per °C for this particular experiment.

In order to establish whether temperature effects are significant in this regard, we start with the premise that one can equate the ice mass directly to C''_{PEAK} at the beginning of the primary drying stage when the amount of ice is known. The amount of ice sublimed is assumed proportional to the reduction in C''_{PEAK} at any point in time. However, we also know that if the temperature is ramped from −51 °C to −30 °C then the impact on the initial value of C''_{PEAK} will be ~ 0.70% (per degree celcius) as shown in Figure 12b. Taking the example of an initial ice mass of 2.5 g per vial, then if the product temperature prior primary drying is −40 °C but the sublimation of ice causes the temperature drop to −43 °C over a period of 15 min (0.25 h) then that 3 °C reduction in temperature alone would decrease C''_{PEAK} by 2.1%. Therefore, it would seem that 2.1% of the ice mass is lost within 15 min leading to an uncertainty of sublimation rate of $(2.5 \times 0.021) \times (60/15) = 0.21$ g·h^{-1}.

If the temperature dependency of C''_{PEAK} remains uncorrected then it is clear that there is significant potential for introducing errors into the estimates for sublimation rate, from using the uncompensated values alone.

A method for compensating C''_{PEAK} for temperature was developed and reported in Smith et al. [19]. The method is based on a compensation factor (Φ) that normalizes all values of C''_{PEAK} to that which would be observed if primary drying proceeded at the initial temperature (T_{ref}) (Equation 2).

$$\Phi = \frac{C''_{PEAK}(T)}{C''_{PEAK}(T_{ref})} \qquad \text{Equation 2}$$

Here, $C''_{PEAK}(T)$ and $C''_{PEAK}(T_{ref})$ are the amplitudes of the relaxation process at a temperature (T) and the initial reference temperature (T_{ref}). The reference temperature is taken as the product temperature at the beginning of primary drying at the point when the vacuum was applied. In this work the reference temperature (T_{ref}) was −44 °C.

The temperature dependency of C''_{PEAK} during the re-heating ramp is modelled satisfactory by a 2nd order polynomial; therefore, the temperature compensation factor (Φ) (Equation 2) could be expressed in terms of the polynomial coefficients, as follows:

$$\Phi = \frac{aT^2 + bT + c}{aT_{ref}{}^2 + bT_{ref} + c} \qquad \text{Equation 3}$$

Values of peak amplitude at any time during primary drying ($C''_{PEAK}(t)$) were then adjusted to the C''_{PEAK} values that would be predicted if the drying were to continue at the reference temperature, i.e. at temperature at the beginning of primary drying, by dividing by Φ to give a temperature compensated peak amplitude ($\hat{C}''_{PEAK}$) according Equation 4.

$$\hat{C}''_{PEAK} = \frac{C''_{PEAK}(t)}{\Phi} \qquad \text{Equation 4}$$

The time profiles of the compensated and the uncompensated values of C''_{PEAK} are shown in Figure 13 (solid and dotted lines respectively).

Figure 13a shows the first 9 h of primary drying over which the TVIS parameter $T_{F_{PEAK}}$ appears to provide a reliable assessment of the predicted product temperature. Figure 13b focusses on the first 3 h of that 9 h period. The purpose of this enlarged view is to demonstrate the impact of temperature on the rate of change of C''_{PEAK} with time (dC''_{PEAK}/dt) and therefore the potential for error in the determination of the sublimation rate. The first point to note is that, up to the point at which the shelf temperature is increased (i.e. 1.1 h into primary drying) both C''_{PEAK} and $\hat{C}''_{PEAK}$ decrease at an approximately linear rate although the C''_{PEAK} profile is not as regular as the $\hat{C}''_{PEAK}$ profile. The second point to note is that the average gradient of C''_{PEAK} is ~20% greater than that of $\hat{C}''_{PEAK}$ (compare arrows A and B in Figure 13b) and hence the same percent error would be expected if sublimation rate were calculated from the uncorrected values of C''_{PEAK}.

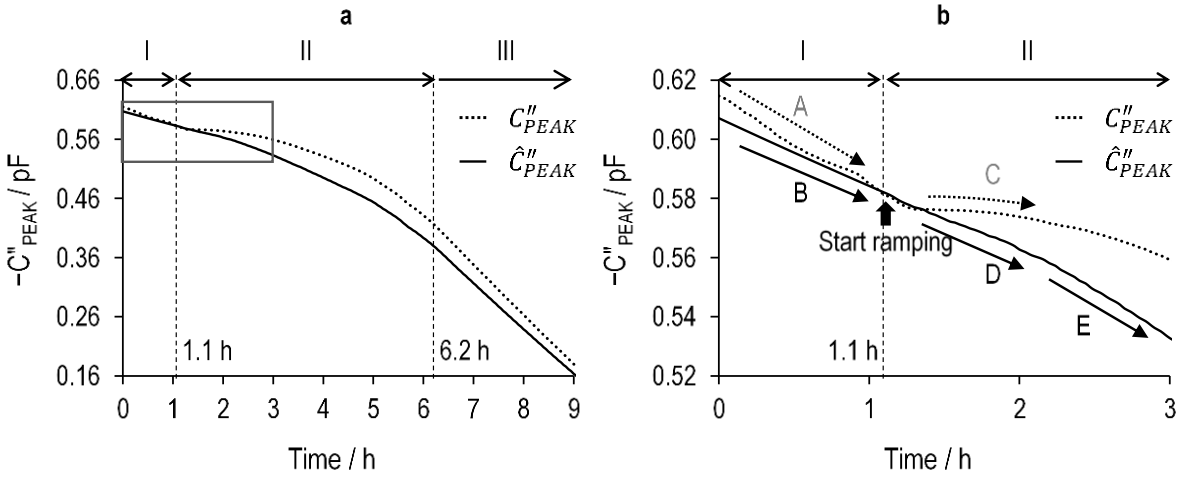

Figure 13 Primary drying profiles of the peak magnitude before and after temperature correction (C''_{PEAK} and $\hat{C}''_{PEAK}$, respectively). (a) profile for the first 9 h of primary drying and (b) close up of the first 3 h. The various steps of primary drying are: Period I Holding at −40 °C; Period II Ramping temperature from −40 to −10 °C at 0.1 °C·min^{-1}; and Period III Holding at −10 °C. Note that the standardization temperature (T_{ref}) used for compensating for the temperature dependency of C''_{PEAK} is −44 °C. Five arrows marked A, B, C, D and E run parallel to the data in order to demonstrate the relative differences in gradient between the uncompensated and compensated values of C''_{PEAK} both before the onset of the temperature ramp (A and B, respectively) and after the temperature ramp (C, D and E, respectively). Before ramping, the surrogate sublimation rate (from dC''_{PEAK}/dt) is higher for the uncompensated values (before the temperature ramp) but almost reduces to zero immediately after the temperature ramp. The implication might be that the sublimation rate is slowing); whereas the compenstated values continue at the same apparent sublimation rate as before the temperature ramp. Then as the temperature continues to ramp the apparent drying rate for the compensated values begins to increase (arrow E) as one might expect.

An average predicted product temperature ($T_{F_{PEAK}}$) of −44.3 ± 0.3 °C was recorded during the initial 0 - 1.1 h period of primary drying (Period I of Figure 13). From the decrease in $\hat{C}''_{PEAK}$ during the

holding period (Period I of Figure 13) one must conclude that sublimative drying has been initiated, presumably because as a result of a combination of three factors: (i) the partial vapour pressure of water is much lower than the total pressure, and the ratio between the two pressures will be maintained during depressurization. For instance, at 20 °C and atmospheric pressure, the partial vapour pressure of water in air would be 23.3 mbar, then on depressurization reduce to 291 µbar. Then the partial water vapour would reduce proportionally to 6.7 µbar, which would be sufficient to promote sublimation (i.e. −44.3 °C has ice vapour pressure of 81 µbar); (ii) a gas diffusion gradient being created between the higher partial pressure of water vapour at the ice surface to the lower partial pressure of water vapour at the condenser; and (iii) the vacuum pump of the freeze dryer could facilitate vapor movement by removing water vapour out of the chamber thereby further promoting drying.

The third and final point to note regarding Figure 13b is that beyond 1.1 h when the shelf temperature and product temperature begins to ramp there is a levelling off in the rate of change of C''_{PEAK} whereas the temperature compensated $\hat{C}''_{PEAK}$ shows a more expected behaviour (arrow E in Figure 13b), i.e. an increase in the rate of change of $\hat{C}''_{PEAK}$ which results from the fact that the sublimation rate will have increased as a consequence of the increased product temperature.

2.5.2 Conversion of $\hat{C}''_{PEAK}$ to ice mass.

Once C''_{PEAK} values have been compensated for its temperature dependence, it is then possible to convert the compensated $\hat{C}''_{PEAK}$ values to ice mass by equating the initial $\hat{C}''_{PEAK}$ value to the initial ice mass in the sensing region of electrode, at the point when the vacuum was applied.

The initial ice content in the frozen mass within the sensing region of the electrode is determined in four steps. The first step is to estimate the quantity of solute and water in the total fill weight of solution (Equation 5 and Equation 6, respectively).

$$Solute\ (g) = \frac{Conc.solution\ (\%w/v) \times Filling\ weight.}{100\ \times Density\ of\ solution} \qquad \text{Equation 5}$$

$$Total\ water\ (g) = Filling\ weight\ - Solute\ (g) \qquad \text{Equation 6}$$

From the literature [31] the density of the 5% w/w lactose solution was taken to be 1.0173 g·mL^{-1} at 20 °C and so the amounts of solute and water were estimated as 0.15 and 2.95 g respectively for a sample weight of 3.1 g.

The second step is the calculation of the total weight of unfrozen water in the vial. By using the concentration of the amorphous solute in the unfrozen fraction (known as maximum freeze concentration, C_g') then the mass of unfreezable water can be estimated as follows:

$$Unfrozen\ water\ (g) = \frac{100 \times Solute\ (g)}{C_g'} \qquad \text{Equation 7}$$

In the case of disaccharides C_g' is approximately equal to 80% w/w [32,33] and so the unfrozen water was estimated at 0.19 g.

The third step is to estimate how much of the total water would convert to ice by subtracting the unfreezable water (Equation 7) from the total amount of water (Equation 6) according Equation 8.

$$m_t\ (g) = Total\ water\ (g) - Unfrozen\ water\ (g) \qquad \text{Equation 8}$$

It follows that for a fill weight of 3.1 g, the amount of ice that can be sublimed during primary drying (m_t) is 2.76 g.

The fourth step is to calculate the portion of the total amount of ice (2.76 g) that occupies the sensing region of the electrode (m_{RE}) and therefore contributes to the magnitude of $\hat{C}''_{PEAK}$. Given that 3.1 g of 5% w/v lactose solution corresponses to the total ice layer height (h_t) of 9 mm including the ice layer height within the electrode region (h_{RE}) and therefore the estimated ice mass bounded by the electrodes height of 7 mm (Ø = 0.7) would be $2.76 \times (7\ mm/9\ mm) = 2.15\ g$. Figure 14 shows the distribution of ice mass between the sensing region (m_{RE}) and the dead zone below the electrodes (m_{BE}), i.e. 2.15 g and 0.61 g respectively. For equating $\hat{C}''_{PEAK}$ to ice mass,we based on the assumption that $\hat{C}''_{PEAK}$ is directly proportional to the amount of ice over a range of fill factors from 0 to 1 and that any ice below the bottom of the electrode has negligible contribution to $\hat{C}''_{PEAK}$.

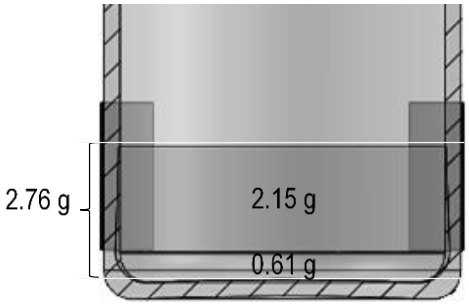

Figure 14 An illustration of ice mass in different regions at initial of primary drying. Approximate 2.15 g of the calculated initial ice (2.76 g) occupies electrode region.

Once the initial ice content in the sensing region of the electrodes has been determined then the residual ice mass within the electrode sensing region (m_{RE}), at any time point (t) during sublimation, can be calculated using TVIS derived parameter $\hat{C}''_{PEAK}$ and thus the estimated values of $m_{RE}(t)$ can be defined as $m_{\hat{C}''_{PEAK}}(t)$ (Equation 9)

$$m_{\hat{C}''_{PEAK}}(t) = m_{RE}(0) \times \frac{\hat{C}''_{PEAK}(t)}{\hat{C}''_{PEAK}(0)} \qquad \text{Equation 9}$$

Where $m_{RE}(0)$ and $\hat{C}''_{PEAK}(0)$ are the ice mass within electrode region (2.15 g) and the compensated C''_{PEAK} (0.615 pF) at the time where the vaccum is applied (0 h of primary drying), respectively. The $\hat{C}''_{PEAK}(t)$ is the compensated value of C''_{PEAK} at any time during primary drying.

Finally, the total ice mass remaining within the vial during the sublimation process is calculated by adding the ice mass in the dead zone below the electrode to TVIS estimated ice mass (Equation 10).

$$m_t(t) = m_{BE} + m_{\hat{C}''_{PEAK}}(t) \qquad \text{Equation 10}$$

Here, the amount of ice below the electrode is 0.61 g.

2.6 Primary drying rate determination

Any change in the ice mass due to sublimation can then be converted directly into sublimation rate ($dm_{\hat{C}''_{PEAK}}/dt$) by using the gradient of the ice mass in time profile (Equation 11). Both the residual ice mass (calculation from Equation 10) and the sublimation rate (calculation from Equation 11) are shown in Figure 15

$$\frac{dm_{\hat{C}''_{PEAK}}}{dt} = -\frac{m_t\ (t_n) - m_t\ (t_{n+1})}{t_n - t_{n+1}} \qquad \text{Equation 11}$$

where t_n and t_{n+1} are consecutive measurement time for the n^{th} and $(n+1)^{th}$ data points.

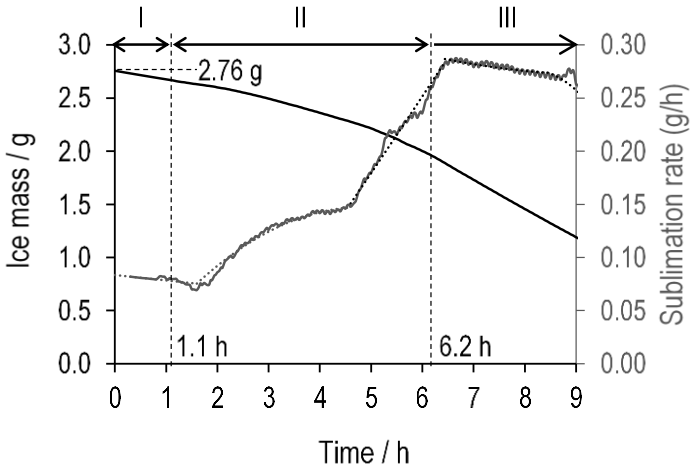

Figure 15 Ice mass contained in the vial (black solid line) and sublimation rate ($dm_{\hat{C}''_{PEAK}}/dt$) (grey solid line) over 9 h of primary drying process are estimated from the standardized $\hat{C}''_{PEAK}$. The different stages of primary drying are presented as period I, II and III for the hold period at −40 °C, the re-heating stage from −40 to −10 °C, and the hold period at −10 °C, respectively.

We note that the application of the linearity principle between $\hat{C}''_{PEAK}$ and ice mass over the region of fill factors of 0 to 1 only holds true if the ice cylinder reduces in height without any appreciable changes in the contact with inside walls of the vial and without any changes in the shape of the ice interface. Given our earlier consideration of the uncertainties in the measurement of TVIS data (See Section 2.5) our estimates for residual ice mass is restricted to the time 9 h period from the beginning of primary drying, during which time we consider that the loss of contact with the glass wall is negligible.

2.7 Estimation of the ice height and the dry layer thickness

A simplified approach for determining the ice layer height during primary drying is to make the assumption that ice interface is flat (in the other words, without a cone-shaped at ice front). Like the determination of ice mass, the ice layer height in the region bounded by the electrode at any time of drying period ($h_{RE}\ (t)$) could be also estimated from the compensated values for the peak amplitude ($\hat{C}''_{PEAK}$) by multiplying this compensated value at any time ($\hat{C}''_{PEAK}\ (t)$) by the ratio of the initial ice layer height bounded in electrode area ($h_{RE}\ (0)$) to the initial value of $\hat{C}''_{PEAK}$ at beginning

of primary drying ($\hat{C}''_{PEAK}\ (0)$) (Equation 12). Since the estimated ice layer height within the electrode region is calculated from the temperature compensated peak amplitude, the predicted values of $h_{RE}\ (t)$ during primary drying is approximately equal to $h_{\hat{C}''_{PEAK}}(t)$. In this work, the value of the initial ice layer height in the region bounded by the electrode ($h_{RE}\ (0)$) is 7 mm.

$$h_{\hat{C}''_{PEAK}}(t) = h_{RE}\ (0) \times \frac{\hat{C}''_{PEAK}\ (t)}{\hat{C}''_{PEAK}\ (0)} \qquad \text{Equation 12}$$

As drying proceeds, the development of dry layer is synchronized with the reduction in the ice layer height in the region bounded by the electrodes. Provided the dry layer does not shrink appreciably during primary drying then the dry layer thickness (l_d) may be derived from the reduction in the ice layer height within the electrode region according to Equation 13.

$$l_d(t) = h_{RE}\ (0) - h_{\hat{C}''_{PEAK}}(t) \qquad \text{Equation 13}$$

The dry layer arising simultaneously over 9 h as the ice layer reduces in height is shown in Figure 16.

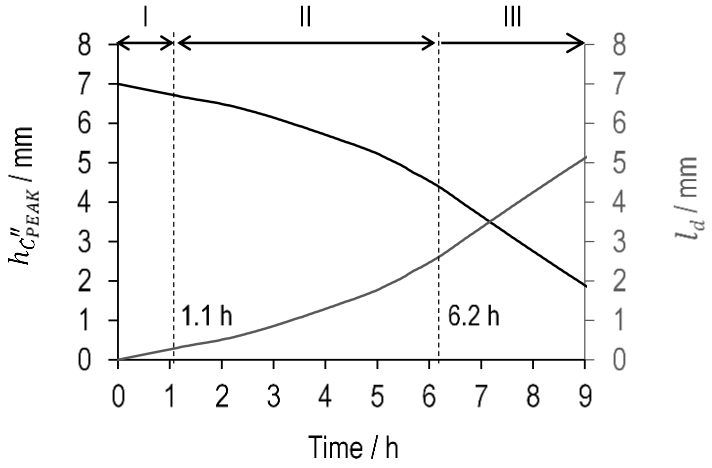

Figure 16 TVIS predicted ice height within the electrode boundary ($h_{\hat{C}''_{PEAK}}$, black solid line) and dry layer thickness (l_d, grey solid line) during the first nine hours of primary drying of 5% w/v lactose.

2.8 Ice interface temperature prediction

Since the sublimation rate and the ice layer height in the region bounded by the electrodes is known, and we have estimates for the ice temperature at the TVIS node, then the next stage is to estimate the temperature at the ice interface as a function of time during primary drying. For that, we

could assume that $T_{F_{PEAK}}$ is to an approximation the same as the ice interface–temperature (T_i). However, given that (i) primary drying induces a temperature gradient in the vertical direction from the ice base (at a higher temperature) to the ice interface at (a lower temperature); and (ii) $T_{F_{PEAK}}$ corresponds to the temperature at the TVIS node; it follows that $T_{F_{PEAK}}$ is likely to record a higher temperature than that which prevails at the ice interface. Two alternatives, more accurate, estimates for determining the ice interface temperature are therefore considered here:

Method I (Figure 17a) is based on the extrapolation from two temperatures at known positions below the ice interface to the position of the ice interface. An analogous methodology has been described in Smith et al. [19] in which a dual electrode pair was used to provide estimate of the two temperatures. In this work in which we have only one electrode pair, we used the product temperature at the base of the vial which is directly inferred from the temperature measured by the thermocouple located at bottom center of the neighboring vial (TC2) and the TVIS-predicted temperature ($T_{F_{PEAK}}$) at the TVIS temperature node (h_n) which positioned at half the height of the ice layer within the electrode region. The height of the TVIS node can be calculate by adding the ice layer height below electrode region (h_{BE}) to the half of ice layer height in electrode region ($h_{\hat{C}''_{PEAK}}(t)/2$) as below:

$$h_n(t) = h_{BE} + \frac{h_{\hat{C}''_{PEAK}}(t)}{2} \qquad \text{Equation 14}$$

The approximate height of the ice layer below the electrode (h_{BE}) is 2 mm.

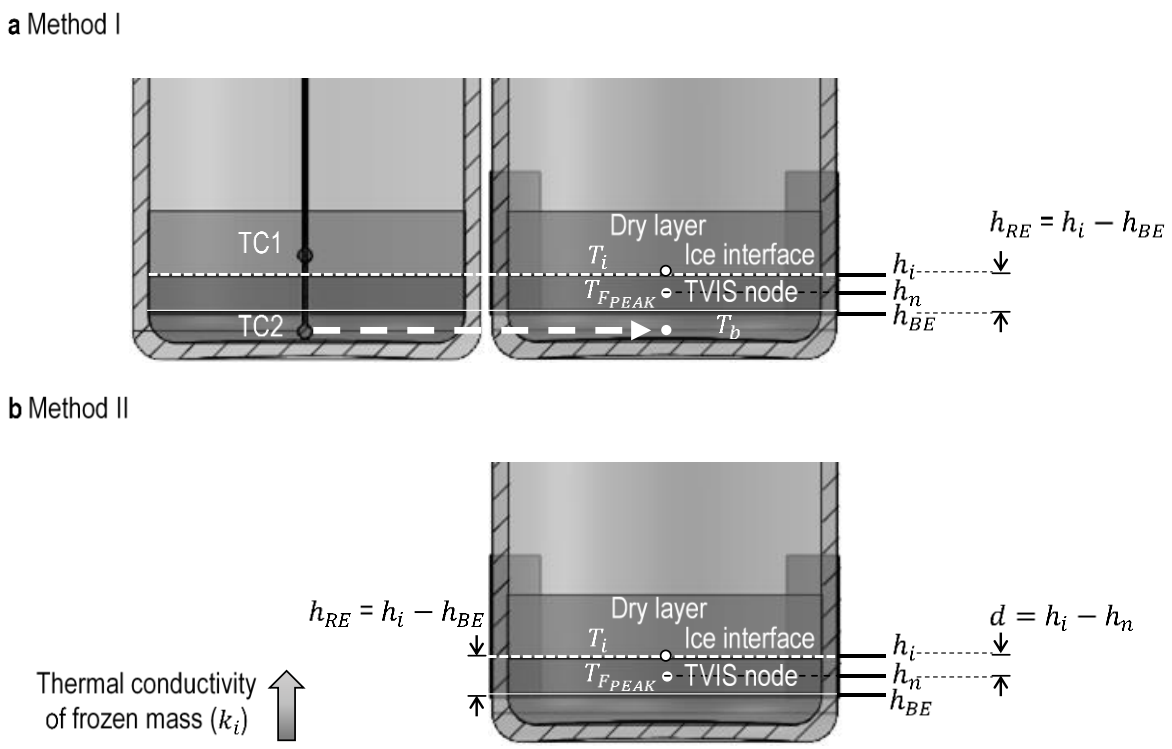

Figure 17 An illustration of the methodology for predicting ice interface temperature a) two-points extrapolation (method I) and b) thermal heat transfer (method II). Note: h_i is the position of the height of ice interface which is equivalent to the sum of the ice layer height within electrode region (h_{RE}) and the ice layer height below the electrode (h_{BE}) and h_n is the height of TVIS node.

Method II (Figure 17b) is based on the principles of heat transfer (dq/dt) through the frozen mass, which depends on the temperature gradient between the region of relatively high temperature at base (T_b) and the relative colder region at the ice interface (T_i) according to the following relationship:

$$\frac{dq}{dt} \propto (T_b - T_i) \qquad \text{Equation 15}$$

The constant of proportionality includes the cross-sectional area inside the vial (A_i), the thickness of the frozen mass (d) and the thermal conductivity of the frozen layer (k_i) and then leads to the expression:

$$\frac{dq}{dt} = \frac{k_i A_i (T_b - T_i)}{d} \qquad \text{Equation 16}$$

Estimates for heat transfer (dq/dt) are determined from the TVIS predicted sublimation rate ($dm_{\hat{C}''_{PEAK}}/dt$) according Equation 17.

$$\frac{dq}{dt} = \frac{dm_{\hat{C}''_{PEAK}}}{dt} \cdot L_i \qquad \text{Equation 17}$$

where L_i is a latent heat of sublimation of ice (679.9 Cal·g^{-1} or 2846 .5 W·s·g^{-1} at −30 °C)

The calculation assumes that heat required to sublime the ice mass from the sublimation interface is derived solely from that supplied by the shelf and percolates in the vertical direction to the interface. This appears to be a reasonable assumption given that we are considering a core vial within the array of vials on the freeze-dryer shelf. In other words, heat flux from the upper shelf down through the stopper and the heat flux from neighboring vials to each side of the TVIS vial are both minimal, in case of the core vials.

Returning to Equation 15 one can see that the heat transfer through the frozen mass (as a driving force for the sublimation) is a function of the temperature difference $(T_b - T_i)$ between two planes. One position is at the ice interface (h_i) which is the sum of the ice layer height bounded by electrodes (h_{RE}) and the additional ice layer height below the electrode (h_{BE}) (Equation 18) and the other, lower position is at the base of the ice layer at a point where the tip of the thermocouple is positioned. However, with the TVIS application this lower position is located at the TVIS sensing node (h_n) and then the temperature difference is given by $T_{F_{PEAK}} - T_i$ (instead of $T_b - T_i$) whereas the distance (d) is that between the ice interface and the sensing node ($h_i - h_n$). By combining Equation 16 and Equation 17, and replacing $T_b - T_i$ and d with the equivalent TVIS parameters, we obtain:

$$h_i(t) = h_{BE} + h_{\hat{C}''_{PEAK}}(t) \qquad \text{Equation 18}$$

$$\frac{dm_{\hat{C}''_{PEAK}}}{dt} \cdot L_i = \frac{k_i A_i \left(T_{F_{PEAK}} - T_i\right)}{h_i - h_n} \qquad \text{Equation 19}$$

Equation 19 is then re-arranged to provide an expression for the ice interface temperature:

$$T_i = T_{F_{PEAK}} - \frac{\frac{dm_{\hat{C}''_{PEAK}}}{dt} \cdot L_i \cdot (h_i - h_n)}{kA_i} \qquad \text{Equation 20}$$

$$T_i = T_{F_{PEAK}} - \frac{\frac{dm_{\hat{C}''_{PEAK}}}{dt} \cdot L_i \cdot \frac{h_{\hat{C}''_{PEAK}}(t)}{2}}{kA_i} \qquad \text{Equation 21}$$

Figure 18 shows the predicted values for $T_{F_{PEAK}}$ along with the results from the two methods for predicting the ice interface temperature (T_i). The inset-plot shown in Figure 18 is a close up of the steady state period during time at which the shelf temperature is kept constant. There you can see that the difference between the predicted ice interface temperature and the temperature at the TVIS node is of the order of 0.5 °C whereas the difference between the predicted T_i from the two methods is negligible.

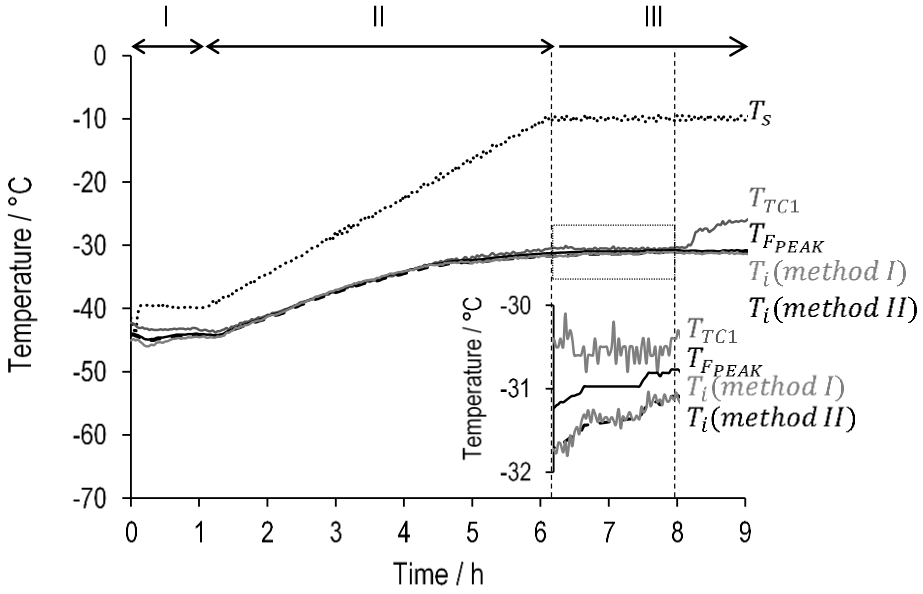

Figure 18 The comparison of ice interface temperature predicted by method I (extrapolating from two-points as demonstrated by Smith et al. [20] and method II (heat transfer equation).

2.9 Dry product resistance determination

The dry layer resistance (R_p) of the product inside a single vial represents the resistance to mass transport (i.e. water vapor flow) from the ice interface through the porous structure within the dry layer to the headspace inside the vial. It is quite simply the constant of proportionality between the driving force for vapour flow (i.e. the pressure differential across the dry layer, ΔP) and the resultant vapour flow rate (i.e. the single vial sublimation rate, dm/dt) can be presented as

$$\Delta P = R_p \cdot \frac{dm}{dt} \qquad \text{Equation 22}$$

The significance of the single vial dry layer resistance is that for any pressure difference across the dry layer (ΔP), the higher the resistance to vapour flow (e.g. from smaller and/or more tortuous pores in the dry layer) the slower the rate of drying.

Re-arranging Equation 22 and re-writing the differential pressure across the dry layer, ΔP, as the difference between the ice interface pressure (P_i) and the headspace ice vapour pressure (P_v) gives:

$$R_p = \frac{(P_i - P_v)}{dm/dt} \quad \text{Equation 23}$$

By considering the geometry of the dry layer in terms of its cross-sectional area and its height, one can instead express the dry layer resistance in terms of its resistivity (ρ_p).

$$R_p = \frac{l_d}{A_i}.\rho_p = \frac{(P_i - P_v)}{dm/dt} \quad \text{Equation 24}$$

where l_d is the dry layer thickness and A_i is the inner horizontal cross-sectional vial area (e.g. 3.82 cm^2 in our case of the 10 mL tubular vial, VC010-20C supplied by Adelphi-HP).

The dry layer resistivity is an intrinsic property associated with the size distribution, tortuosity and connectivity of the pores left behind once the ice has been sublimed and/or any cracks through or around the dry layer. In other words, anything that hinders or facilitates vapor flux from the ice interface to the headspace in the vial. Factors affecting the ρ_p range from formulation additives [34,35] to the freezing behavior of the solution [36-39] including the application of controlled nucleation, given the impact of these factors on the amount of ice that forms and the size distribution of the ice crystals [40,41].

By re-arranging Equation 24 in terms of sublimation rate, it was demonstrated clearly that the larger the internal cross-sectional area of the vial the faster the product will dry (sublimation rate $\propto$ the area of the horizontal cross section of sample).

$$\frac{dm}{dt} = \frac{A_i}{l_d}.\frac{(P_i - P_v)}{\rho_p} \quad \text{Equation 25}$$

It is common practice to normalize for any differences in cross sectional area (in order to make comparisons between products and processes) and in particular when batch-drying rates are determined using techniques such as MTM and TDLAS, where mass transport originates from many vials. This is achieved by multiplying Equation 24 by the area, whether that is the inner cross section

area of a single vial (in the case of our TVIS measurements) or the collective inner cross-sectional area of the multiple vials in a batch (in the case of MTM or TDLAs measurements).

$$\hat{R}_\rho \ = l_d.\rho_p \ = A_i \frac{(P_i - P_v)}{dm/dt} \qquad \text{Equation 26}$$

Where $\hat{R}_\rho$ is known as the area normalized mass transfer resistance. It is clear from Equation 26 that $\hat{R}_\rho$ will increase as the dry layer increases in height (l_d) provided there are no structural changes in the dry layer that might affect its resistivity (ρ_p). This would hold true in cases where the ice crystal structure is uniform in the vertical direction of the vial and where the dry layer remains stable; in other words, the dry layer is not subject to shrinkage nor any internal collapse of the pore structure. This second condition is often (but not always) achievable if the product is dried well below its collapse temperature.

In practical terms, the application of Equation 26 to our TVIS measurements can be realized if we use $\hat{C}''_{PEAK}$ derived estimates for both the single vial sublimation rate ($dm_{\hat{C}''_{PEAK}}/dt$) (Section 2.6) and the dry layer thickness (l_d) at time t (section 2.7), and F_{PEAK} derived estimates for the ice interface temperature, T_i, (Section 2.8) and therefore the partial pressure of ice at the sublimation front, P_i.

The only remaining parameter for consideration is the partial pressure of ice inside the headspace of the vial (P_v). Often one can assume that P_v is the same as the partial pressure of ice vapour inside the chamber, P_c, because there is negligible pressure drop across the vent in the stopper (known as the stopper resistance, R_s). In those cases, P_c is measured by a calibrated Pirani gauge, for example, or calculated from models used in the MTM and TDLAS techniques [29,42,43]. However, the Virtis Advantage Plus used in this work does not have a water vapour pressure sensor, nor is equipped with MTM or TDLAS, and so we must predict P_c from the partial vapour pressure at the sink, in the other words use the temperature of the internal condenser (P_{cd}). Fortunately, the condenser is not separated from the chamber by a duct and is close to product (i.e. condenser is installed inside

chamber under the bottom freeze drying shelf) and so there will be no other pressure drop along the path between the vials and the ice trap.

It follows that the two pressures required for the calculation of the dry layer resistance are obtained from the respective temperatures at the ice interface and the condenser. To that end we have used the form of the Clausius–Clapeyron equation as reported by Murphy and Koop [44].

$$P_i = e^{(28.9074-\left(\frac{6143.7}{T_i}\right))} \quad \text{Equation 27}$$

$$P_{cd} = e^{(28.9074-\left(\frac{6143.7}{T_{cd}}\right))} \quad \text{Equation 28}$$

where P_i and P_{cd} are the partial pressures of ice in Pascal (Pa) at the ice interface and condenser, respectively (1 Pa = 0.0075 Torr) and T_i and T_{cd} are corresponding temperatures in Kelvin (K)

By replacing the sublimation rate and P_v with the equivalent TVIS derived parameters and P_{cd} into Equation 26, the final expression for the area-normalized dry layer resistance is:

$$\hat{R}_\rho \ = l_d . \rho_p \ = A_i \frac{(P_i - P_{cd})}{dm_{\hat{C}''_{PEAK}}/dt} \quad \text{Equation 29}$$

In this experiment, $\hat{R}_\rho$ started at a value of ~ 124.4 kPa·m^2·s·kg^{-1} (2.59 Torr·cm^2·h·g^{-1}) rather than zero, presumably because of a skin on the dry product as descibed by Pikal [4]. During the ramp phase (period II in Figure 19) the shelf temperature was raised from −40 to −10 °C at 0.1 °C·min^{-1}. In this phase, $\hat{R}p$ increased as the dry layer developed in thickness, up to 4.5 h. At that point, the product temperature at ice interface (T_i) had reached ~ −33.3 °C, and the overall resistance started to decrease from the maximum value of 242.3 kPa·m^2·s·kg^{-1} (5.05 Torr·cm^2·h·g^{-1}) to a value of 162.7 kPa·m^2·s·kg^{-1} (3.39 Torr·cm^2·h·g^{-1}).

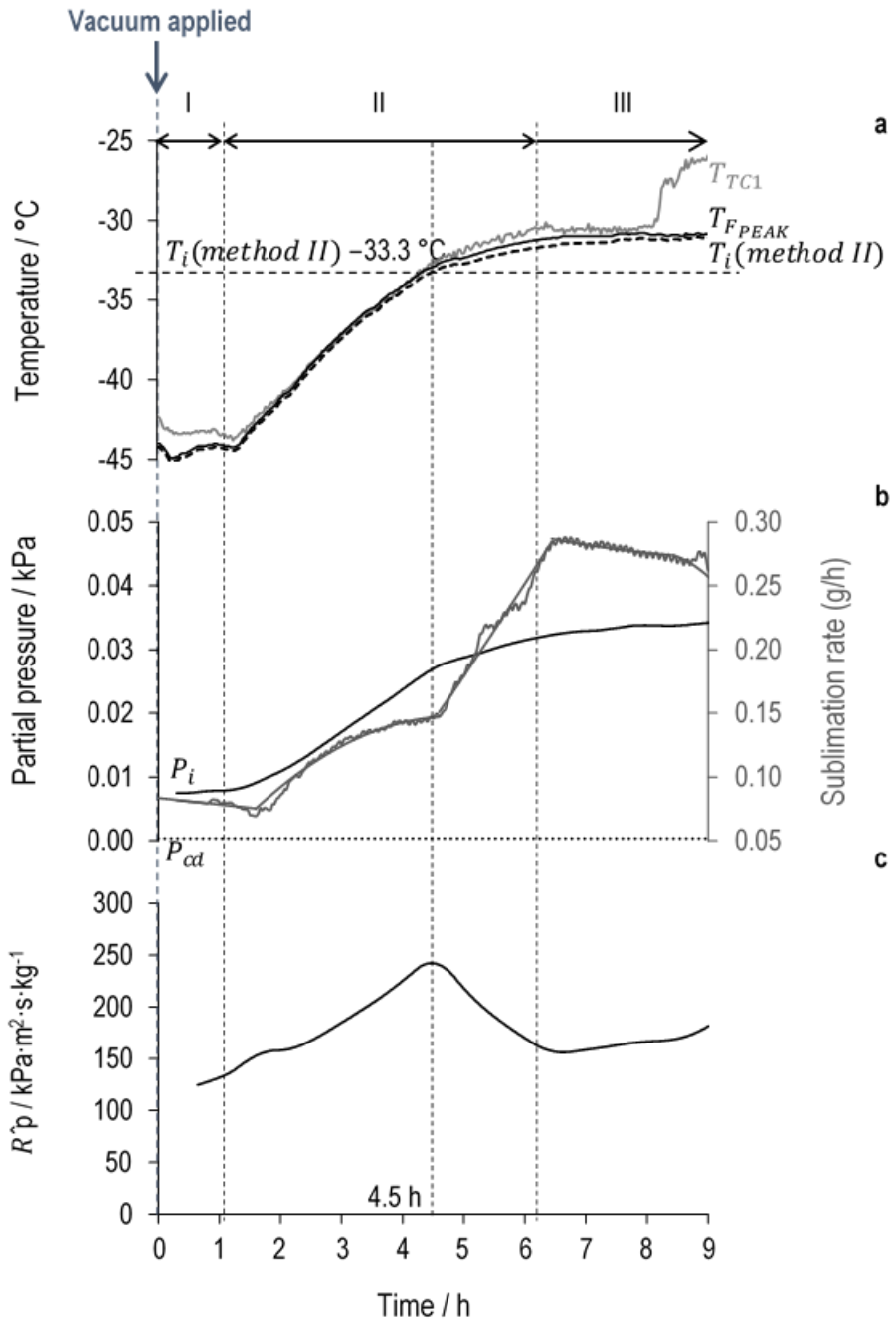

Figure 19 Results of 5% w/v lactose during the first 9 h of primary drying stage (a) the thermocouple temperature profile (T_{TC1}, grey solid line), TVIS predicted temperature ($T_{F_{PEAK}}$, black solid line) and the calculated ice interface temperature from method II (T_i, black dash line); (b) Ice partial pressure at the sublimation front (black solid line) and condenser (black dot line), and sublimation rate (grey solid line) over the drying period; (c) product resistance ($\hat{R}_\rho$, black solid line). Period I, II and III denote the 1st hold period of 1.1 h after the applying of the vacuum, the shelf temperature ramp from −40 to −10 °C over a period of 5.1 h , and the 2nd hold period of primary drying, respectively. When the ice temperature at the sublimation front reaches −33.3 °C (horizontal black dashed line) the dry product resistance start to decrase which indicates the begining of a microcollapse event.

This observation suggests that the freeze-dried cake is probably at the beginning of a collapse event; in which the sublimation rate increases as a consequence of the fusion of the pores in the dry

layer, thereby reducing the dry layer resistance. In order to quantify this sugestion we then plotted the dry layer resistance as a function of dry layer height (Figure 20) and compared that to the SEM image taken from the cake at the end of the process (Figure 21). The larger pore size and possible cake shrinkage at the edges was seen in the dried layer at depths of greater than 1.51 mm.

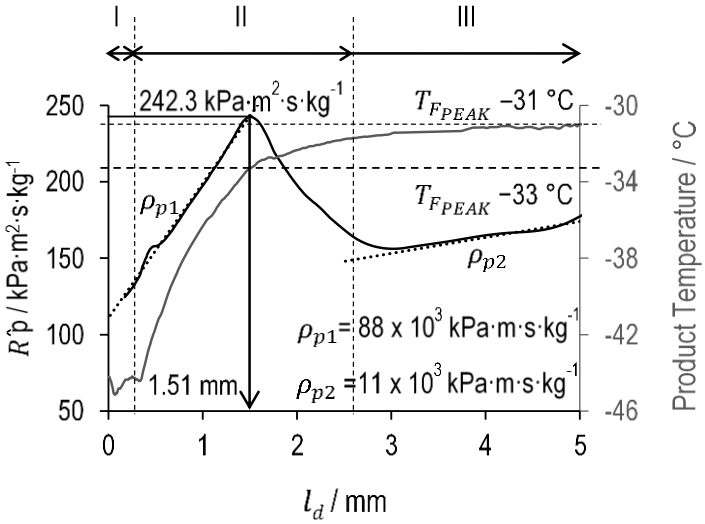

Figure 20 The dry product resistance ($\hat{R}_\rho$, black solid line) and the TVIS-predicted ice interface temperature T_i (grey solid line) as a function of dry layer thickness for lactose freeze dried from a 5% w/v solution (over the first 8.87 h of primary drying). Period I, II and III are holding at −40 °C ($T_{F_{PEAK}}$−44.3± 0.31 °C), re-heating from −40 to −10 °C (0.1 °C·min^{-1}), and holding at −10 °C, respectivly. A product resistance starts to decrease continuously after product temperature (T_i) reaches −33 °C corresponding to dry layer thickness of 1.51 mm.

Once the shelf temperature had stabilized at −10 °C (Period III in Figure 19 and Figure 20), the product temperature predicted from TVIS parameters was almost constant at −30.6 ± 0.1 °C due to a nearly constant sublimation rate. During this hold period, $\hat{R}_\rho$ increased at a much slower rate than was observed in the region II.

As the dry layer increases above 3 mm (Figure 20) the magnitude of $\hat{R}_\rho$ is incomparable to that observed prior to the collpase event, however, the gredient of dotted lines ρ_{p1} and ρ_{p2} illustrate the siginificant difference between the dry layer resistivity of the non-collapsed and microcollapsed product, which are 88 and 11 MPa·m·s·kg^{-1} respectively.

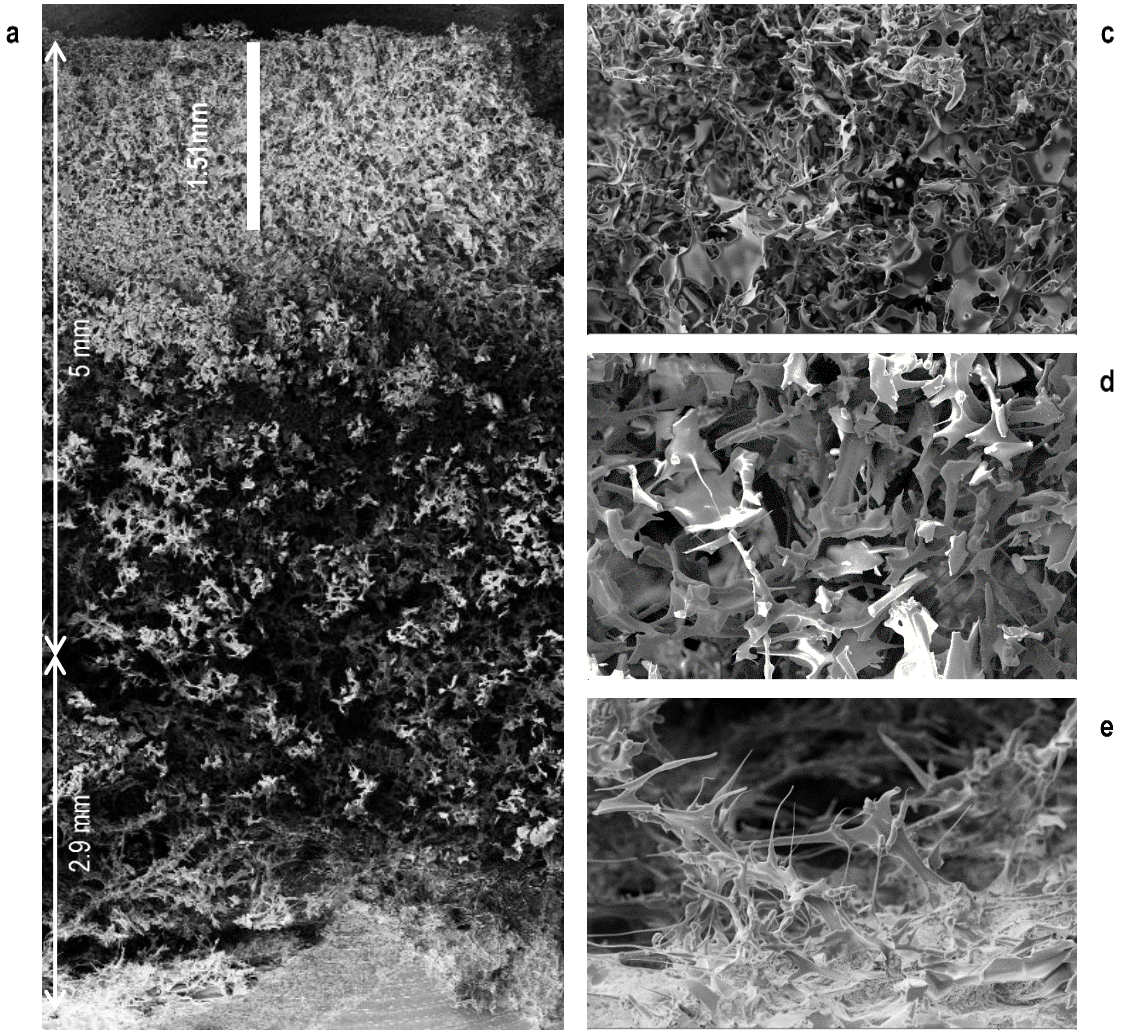

Figure 21 Scanning electron photomicrographs of a freeze-dried cake of 5% w/v lactose at the end of cycle. (a) an overview of a vertical cross section of freeze-dried cake at a magnification of 25x and (b-d) a morphology of the dried layer at a magnification of 500x (b) top, (c) middle, and (d) bottom.

With our TVIS approach, one could use C''_{PEAK} for determining drying rate and subsequently the dried product resistance without the impact from a shrinkage of the freeze-dried cake at the onset of the collapse because the dielectric loss peak that TVIS measures relates directly to the dielectric relaxation of ice rather than the dried product. However, only one concern regarding this technique is the requirement for the ice layer to be intimately contact with the glass wall. Loss of the ice contact with glass wall can introduce an uncertainty in drying rate determination as described by Smith et al. [19]

2.10 Impact of collapse on the sublimation rate

Some additional observations are now made regarding the impact of the collapse event. At 4.5 h of primary drying where the product temperature was just below −33 °C, a significant increase in sublimation rate was observed (from 0.08 to 0.28 g·h^{-1}) as the ice interface temperatrure was increased to −30 °C and the dry product resistance ($\hat{R}_\rho$) decreased (Figure 19b and Figure 19c). Assuming that each drying rate applied was observed for the entire primary drying phase then the predicted drying times at product temperatures ($T_{F_{PEAK}}$) of −44.3 ± 0.31 °C for the non-collapsed product and −30.9 ± 0.11 °C for the microcollapsed product would be 34 and 10 h which is almost a 3.5 fold decrease (associated with the higher temperature and the lower dry layer resistance). Aside from these numerical observations, the partially collapsed status of the freeze-dried cake could not be discerned simply from the visual appearance of the cake but rather this condition could only be confirmed by SEM images recorded at the end of the process. Our inference is that TVIS measurements could be used as an indirect assessment of the phenonemon of micro-collapse.

Conclusion

This work has introduced methods for the analysis of the imaginary capacitance spectrum of a TVIS vial filled with a 5% lactose solution, for monitoring the primary drying stage of the freeze-drying cycle. The two primary parameters extracted from the TVIS spectrum were the peak amplitude and the peak frequency (C''_{PEAK} and F_{PEAK}) associated with the dielectric relaxation of ice.

The peak frequecy (F_{PEAK}) provided a measurement of the temperature ($T_{F_{PEAK}}$) at the TVIS node while a temperature-compensated value of the peak amplitude ($\hat{C}''_{PEAK}$) provided an estimated of the ice mass from which the sublimation rate ($dm_{\hat{C}''_{PEAK}}/dt$) was calculated. Since in this study, only one pair of electrodes was used then we were not able to use exactly the same method that was used in the dual electrode system for determining the sublimation rate and the ice interface temperature [19]. In this new study, $\hat{C}''_{PEAK}$ was also used to determine the position of the ice interface from the bottom of the vial (h_i) from which a simple method for determinining the thickness of the dry layer

was also developed. For determining the ice interface temperature, two alternative methods were developed (section 2.8) based on combinations of the temperature at the base of the ice layer in the nearest neighbout vial (T_b) and the ice temperature at the TVIS node ($T_{F_{PEAK}}$), height of the ice interface (h_i), height of the TVIS node (h_n), and the TVIS derived parameters for heat transfer ($dm_{\hat{C}''_{PEAK}}/dt$).

There are four lessons to be taken from this study: (i) From the discontinuity in the increase in sublimation rate (during the temperature ramp that was imposed during the primary drying stage) we could indirectly observe the phenomenon of micro-collapse (as confirmed by SEM, at the end of the cycle); (ii) From the determination of the ice interface temperature we were then able to state that the microcollapse event occurred at the same temperature (−33 °C) that was predicted by DSC for the onset of the glass transition; (iii) From our observation on the sublimation rate, before and after micro-collapse, one can expect there would be a four fold reduction in primary drying time, from the opportunity to dry a more porous product at the higher temperature of ~−31 °C as opposed to −43 °C; (iv) From the TVIS derived parameters of product temperature ($T_{F_{PEAK}}$) and sublimation rate ($dm_{\hat{C}''_{PEAK}}/dt$) could be used for calculating the product dry layer resistance (and resistivity) before and after the collapse event.

Acknowledgement

This research received the support from an Innovate UK grant (LyoDEA 100527) for the development of the TVIS system; and the Government Pharmaceutical Organization (GPO), Thailand that provided the funding for the PhD studentship.

Appendix: Fill factor calculation

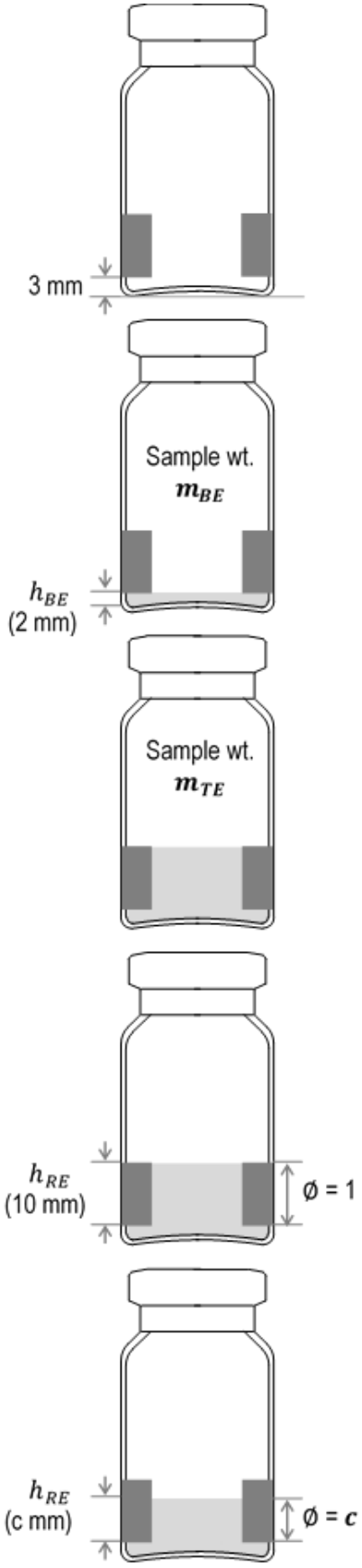

Tare an empty TVIS vial

Note: The height of the lower edge of electrode above the external base of the vial is 3 mm

Add the solution until the volume reaches the lower edge of the electrode and then record the weight of the solution ($\boldsymbol{m_{BE}}$)

Note: The height of sample below the lower edge of electrode from the internal base of the vial (h_{BE}) is 2 mm

Add more of the same solution until the volume reaches the upper edge of electrode and then record the weight of the solution ($\boldsymbol{m_{TE}}$)

Calculate the weight of the solution in the region bounded by the electrode for a fill factor (Ø) of 1:

$$\text{Ø}\,(1) = \boldsymbol{m_{TE}} - \boldsymbol{m_{BE}}$$

Note: The height of the solution bounded by the electrodes is defined as h_{RE}. For fill factor of 1, the value of h_{RE} is 10 mm

Once the individual vial is calibrated for fill factor of 1, then calculate the weight of the solution in the region bounded by electrode for any fill factor of $\boldsymbol{c}$:

$$\text{Ø}\,(\boldsymbol{c}) = [(\boldsymbol{m_{TE}} - \boldsymbol{m_{BE}}) \times \boldsymbol{c}] + \boldsymbol{m_{BE}}$$

Note: For electrode height of 10 mm, the value of h_{RE} is c mm for any fill factor of c

Reference

[1] G. Smith, M.S. Arshad, E. Polygalov, I. Ermolina, T.R. McCoy, P. Matejtschuk, Process understanding in freeze-drying cycle development: applications for through-vial impedance spectroscopy (tvis) in mini-pilot studies, J. Pharm. Innov. 12 (2017) 26-40.

[2] L. Rey, Glimpses into the realm of freeze-drying: classical issues and new ventures. , in: L. Rey, J.C. May (Eds.), Freeze-Drying/Lyophilization of Pharmaceutical and Biological Products., 3rd ed., Informa Healthcare, UK, 2010, pp. 1-28.

[3] Y.H. Roos, Crystallization Collapse and Glass Transition in Low-Water Food Systems, in: D.S. Reid, T. Sajjaanantakul, P.J. Lillford, S. Charoenrein (Eds.), Water Properties in Food, Health, Pharmaceutical and Biological Systems: ISOPOW 10, John Wiley & Sons, 2010.

[4] M.J. Pikal, Use of laboratory data in freeze drying process design: heat and mass transfer coefficients and the computer simulation of freeze drying, J. Parenter. Sci. Technol. 39 (1985) 115-139.

[5] E. Meister, H. Gieseler, Freeze-dry microscopy of protein/sugar mixtures: Drying behavior, interpretation of collapse temperatures and a comparison to corresponding glass transition data, J. Pharm. Sci. 98 (2009) 3072-3087.

[6] R.A. Depaz, S. Pansare, S.M. Patel, Freeze-drying above the glass transition temperature in amorphous protein formulations while maintaining product quality and improving process efficiency, J. Pharm. Sci. 105 (2016) 40-49.

[7] F. Fonseca, S. Passot, O. Cunin, M. Marin, Collapse temperature of freeze-dried lactobacillus bulgaricus suspensions and protective media, Biotechnol. Prog. 20 (2004) 229-238.

[8] M. Mujat, K. Greco, K.L. Galbally-Kinney, D.X. Hammer, R.D. Ferguson, N. Iftimia, P. Mulhall, P. Sharma, M.J. Pikal, W.J. Kessler, Optical coherence tomography-based freeze-drying microscopy, Biomed. Opt. Express. 3 (2012) 55-63.

[9] K. Greco, M. Mujat, K.L. Galbally-Kinney, D.X. Hammer, R.D. Ferguson, N. Iftimia, P. Mulhall, P. Sharma, W.J. Kessler, M.J. Pikal, Accurate prediction of collapse temperature using optical coherence tomography-based freeze-drying microscopy, J. Pharm. Sci. 102 (2013) 1773-1785.

[10] J.C. Kasper, M. Wiggenhorn, M. Resch, W. Friess, Implementation and evaluation of an optical fiber system as novel process monitoring tool during lyophilization, Eur. J. Pharm. Biopharm. 83 (2013) 449-459.

[11] J. Horn, W. Friess, Detection of collapse and crystallization of saccharide, protein and mannitol formulations by optical fibers in lyophilization, Front. Chem. 6 (2018).

[12] G. Smith, M.S. Arshad, K. Nazari, E. Polygalov, I. Ermolina, J. Taylor, T. Page, Through-vial impedance spectroscopy: a new in-line process analytical technology for freeze drying, Pharm. Technol. 38 (2014).

[13] N. Milton, M.J. Pikal, M.L. Roy, S.L. Nail, Evaluation of manometric temperature measurement as a method of monitoring product temperature during lyophilization, PDA. J. Pharm. Sci. Technol. 51 (1997) 7-16.

[14] S.C. Schneid, R.E. Johnson, M.L. Lewis, P. Stärtzel, H. Gieseler, Application of process analytical technology for monitoring freeze-drying of an amorphous protein formulation: Use of complementary tools for real-time product temperature measurements and endpoint detection, J. Pharm. Sci. 104 (2015) 1741-1749.

[15] G. Smith, M.S. Arshad, E. Polygalov, I. Ermolina, Factors affecting the use of impedance spectroscopy in the characterisation of the freezing stage of the lyophilisation process: the impact of liquid fill height in relation to electrode geometry, AAPS PharmSciTech 15 (2014) 261-269.

[16] G. Smith, M.S. Arshad, E. Polygalov, I. Ermolina, Through-vial impedance spectroscopy of the mechanisms of annealing in the freeze-drying of maltodextrin: the impact of annealing hold time and temperature on the primary drying rate, J. Pharm. Sci. 103 (2014) 1799-1810.

[17] M.S. Arshad, G. Smith, E. Polygalov, I. Ermolina, Through-vial impedance spectroscopy of critical events during the freezing stage of the lyophilization cycle: the example of the impact of sucrose on the crystallization of mannitol, Eur. J. Pharm. Biopharm. 87 (2014) 598-605.

[18] G. Smith, M.S. Arshad, E. Polygalov, I. Ermolina, An application for impedance spectroscopy in the characterisation of the glass transition during the lyophilization cycle: the example of a 10% w/v maltodextrin solution, Eur. J. Pharm. Biopharm 85 (2013) 1130-1140.

[19] G. Smith, Y. Jeeraruangrattana, I. Ermolina, The application of dual-electrode through vial impedance spectroscopy for the determination of ice interface temperatures, primary drying rate and vial heat transfer coefficient in lyophilization process development, Eur. J. Pharm. Biopharm. 130 (2018) 224-235.

[20] G. Smith, E. Polygalov, Chapter 11 Through vial impedance spectroscopy (TVIS): A novel approach to process understanding for freeze-drying cycle development, in: K.R. Ward, P. Matejtschuk (Eds.), Lyophilization of Pharmaceuticals and Biologicals: New Technologies and Approaches, 1st ed., Humana Press, New York, 2019, pp. 241-290.

[21] P. Gabbott, A practical introduction to differential scanning calorimetry, in: A practical introduction to differential scanning calorimetryPrinciples and Applications of Thermal Analysis, Blackwell Publishing, Singapore, 2008, pp. 1-50.

[22] E. Meister, H. Gieseler, A significant comparison between collapse and glass transition temperatures, Epr (2008) n.k.

[23] L.M. Her, R.P. Jefferis, L.A. Gatlin, B. Braxton, S.L. Nail, Measurement of glass transition temperatures in freeze concentrated solutions of non-electrolytes by electrical thermal analysis, Pharm. Res. 11 (1994) 1023-1029.

[24] K.R. Ward, P. Matejtschuk, The use of microscopy, thermal analysis, and impedance measurements to establish critical formulation parameters for freeze-drying cycle development., in: L. Rey, J.C. May (Eds.), Freeze Drying/Lyophilization of Pharmaceutical and Biological Products, 3rd ed., Informa Healthcare, London, 2010, pp. 111-135.

[25] G.P. Johari, E. Whalley, The dielectric properties of ice Ih in the range 272–133 K, J. Chem. Phys. 75 (1981) 1333-1340.

[26] I. Popov, I. Lunev, A. Khamzin, A. Greenbaum, Y. Gusev, Y. Feldman, The low-temperature dynamic crossover in the dielectric relaxation of ice I h, Phys. Chem. Chem. Phys. 19 (2017) 28610-28620.

[27] S. Hibler, C. Wagner, H. Gieseler, Vial freeze-drying, part 1: New insights into heat transfer characteristics of tubing and molded vials, J. Pharm. Sci. 101 (2012) 1189-1201.

[28] B. Scutella, S. Passot, E. Bourles, F. Fonseca, I.C. Trelea, How vial geometry variability influences heat transfer and product temperature during freeze-drying, J. Pharm. Sci. 106 (2017) 770-778.

[29] M.J. Pikal, M.L. Roy, S. Shah, Mass and heat transfer in vial freeze-drying of pharmaceuticals: Role of the vial, J. Pharm. Sci. 73 (1984) 1224-1237.

[30] L.G. MacDowell, C. Vega, Dielectric constant of ice ih and ice v: A computer simulation study, J. Phys. Chem. B. 114 (2010) 6089-6098.

[31] E.J. McDonald, A.L. Turcotte, Density and refractive indices of lactose solutions, J. Res. Natl. Bur. Stand. 41 (1948) 63-68.

[32] J. Liesebach, T. Rades, M. Lim, A new method for the determination of the unfrozen matrix concentration and the maximal freeze-concentration, Thermochim. Acta. 401 (2003) 159-168.

[33] M. Xu, G. Chen, C. Zhang, S. Zhang, Study on the unfrozen water quantity of maximally freeze-concentrated solutions for multicomponent lyoprotectants, J. Pharm. Sci. 106 (2017) 83-91.

[34] D.E. Overcashier, T.W. Patapoff, C.C. Hsu, Lyophilization of protein formulations in vials: Investigation of the relationship between resistance to vapor flow during primary drying and small-scale product collapse, J. Pharm. Sci. 88 (1999) 688-695.

[35] R.E. Johnson, M.E. Oldroyd, S.S. Ahmed, H. Gieseler, L.M. Lewis, Use of manometric temperature measurements (MTM) to characterize the freeze-drying behavior of amorphous protein formulations, J. Pharm. Sci. 99 (2010) 2863-2873.

[36] J.A. Searles, J.F. Carpenter, T.W. Randolph, The ice nucleation temperature determines the primary drying rate of lyophilization for samples frozen on a temperature-controlled shelf, J. Pharm. Sci. 90 (2001) 860-871.

[37] A.K. Konstantinidis, W.Y. Kuu, L. Otten, S.L. Nail, R.R. Sever, Controlled nucleation in freeze-drying: Effects on pore size in the dried product layer, mass transfer resistance, and primary drying rate, J. Pharm. Sci. 100 (2011) 3453-3470.

[38] S. Rambhatla, R. Ramot, C. Bhugra, M.J. Pikal, Heat and mass transfer scale-up issues during freeze drying: II. Control and characterization of the degree of supercooling, AAPS PharmSciTech 5 (2004) 54-62.

[39] I. Oddone, R. Pisano, R. Bullich, P. Stewart, Vacuum-induced nucleation as a method for freeze-drying cycle optimization, Ind Eng Chem Res 53 (2014) 18236-18244.

[40] H. Goshima, G. Do, K. Nakagawa, Impact of Ice Morphology on Design Space of Pharmaceutical Freeze-Drying, Journal of Pharmaceutical Sciences 105 (2016) 1920-1933.

[41] A. Arsiccio, A.A. Barresi, R. Pisano, Prediction of ice crystal size distribution after freezing of pharmaceutical solutions, Crystal Growth & Design 17 (2017) 4573-4581.

[42] W.Y. Kuu, K.R. O'Bryan, L.M. Hardwick, T.W. Paul, Product mass transfer resistance directly determined during freeze-drying cycle runs using tunable diode laser absorption spectroscopy (TDLAS) and pore diffusion model, Pharm. Dev. Technol. 16 (2011) 343-357.

[43] B. Scutellà, I.C. Trelea, E. Bourlès, F. Fonseca, S. Passot, Determination of the dried product resistance variability and its influence on the product temperature in pharmaceutical freeze-drying, Eur. J. Pharm. Biopharm 128 (2018) 379-388.

[44] D.M. Murphy, T. Koop, Review of the vapour pressures of ice and supercooled water for atmospheric applications, Q. J. R. Meteorol. Soc 131 (2005) 1539-1565.